iScience

CellPress
OPEN ACCESS

Article

Enabling large-scale production of algal oil in continuous output mode

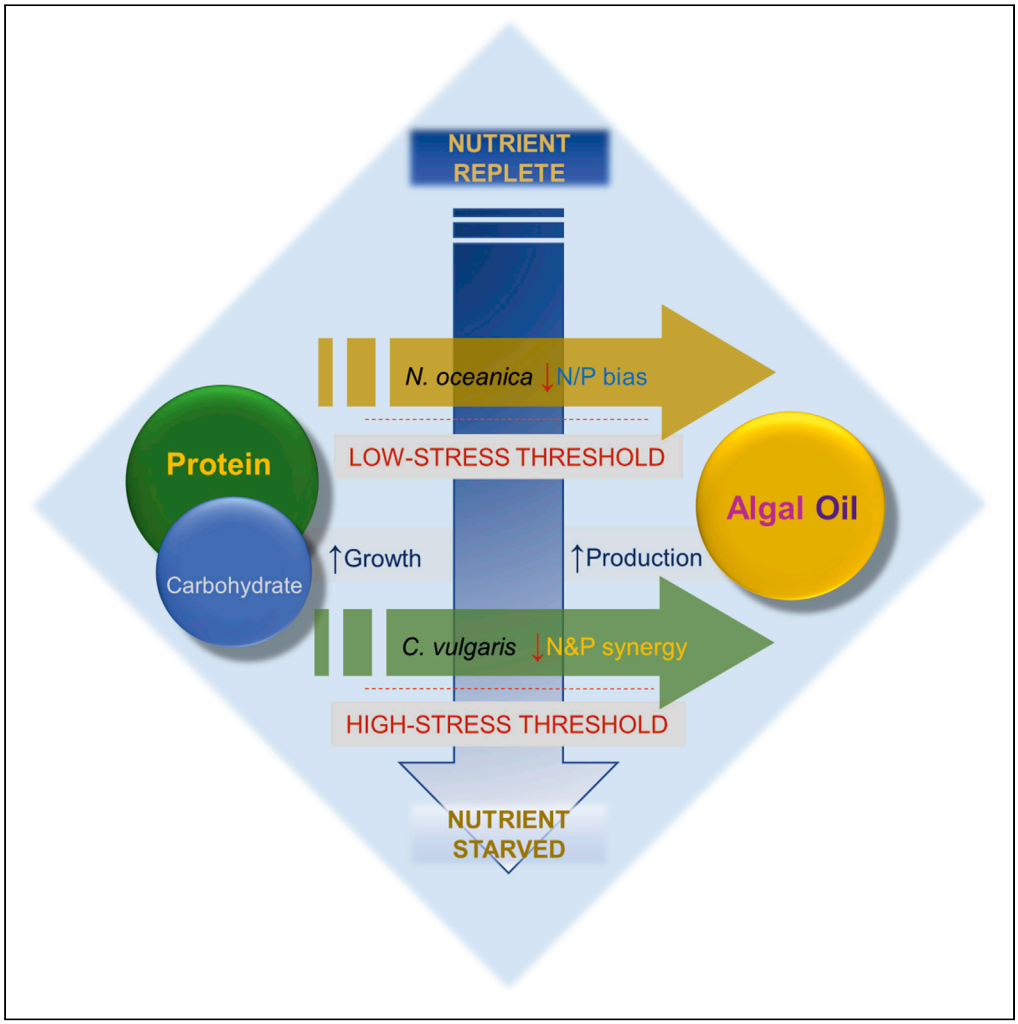

Stephen P. Slocombe, Maria Huete-Ortega, Rahul Vijay Kapoore, ..., John G. Day, Michele S. Stanley, Seetharaman Vaidyanathan

s.vaidyanathan@sheffield.ac.uk

Highlights

Regulatory traits that confer high oil productivity in two algae species were identified

Traits were mostly associated with the oceanic species but not in the estuarine species

Nutrient-depletion thresholds and preferential accumulation differed in the 2 species

Algae type, habitat, and conditions conducive to oil productions are signposted

Slocombe et al., iScience 24, 102743
July 23, 2021
https://doi.org/10.1016/j.isci.2021.102743

iScience

CellPress
OPEN ACCESS

Article

Enabling large-scale production of algal oil in continuous output mode

Stephen P. Slocombe,[1,5] Maria Huete-Ortega,[2,3,5] Rahul Vijay Kapoore,[2,4,5] Katarzyna Okurowska,[2] Alison Mair,[1] John G. Day,[1] Michele S. Stanley,[1] and Seetharaman Vaidyanathan[2,6,*]

SUMMARY

Large-scale algal oil production requires continuous outputs and a trade-off between growth and oil content. Two unrelated marine algae (*Nannochloropsis oceanica* [CCAP 849/10] and *Chlorella vulgaris* [CCAP 211/21A]) that showed high oil production under batch culture were studied under controlled semicontinuous cultivation conditions. Three essential attributes maximized oil productivity: (i) downregulation of cell size to maximize light absorption under N limitation; (ii) low nutrient-depletion thresholds to trigger oil induction; (iii) a means of carbohydrate suppression in favor of oil. *N. oceanica* responded better to input N/P variations and is more suited to continuous oil production. A low N/P ratio was effective in both suppressing carbohydrate and reducing cell size concomitant with oil production. In *C. vulgaris*, nutrient starvation thresholds for oil were higher and carbohydrate was preferentially induced, which impeded stress-level optimization for oil. These differences, which impact continuous oil production at scale, are driven by species adaptation to specific marine habitats.

INTRODUCTION

Renewable energy generation with a conceptually carbon negative process is an attractive proposition for development. In this regard, algal biofuels are worthy of continued attention, provided the question of economic feasibility is addressed and the carbon-negative status can be scaled overall, from well to wheel. Large-scale cultivation of microalgae for renewable oil production has been motivated by high potential yields but somewhat limited by techno-economic challenges (Day et al., 2012; Georgianna and Mayfield, 2012; Greenwell et al., 2010; Mata et al., 2010; Slocombe et al., 2016; Stephens et al., 2010; Wijffels and Barbosa, 2010; Williamsle and Laurens, 2010). Some of the problems now seem tractable, for instance, the high costs of harvesting and dewatering of biomass using flocculation or filtration have decreased (Butler et al., 2021; Danquah et al., 2009; Goswami et al., 2019) or could be bypassed (Tseng et al., 2019). Fertilizer costs can be diminished by medium recycling and by using wastewater inputs (Benemann, 2013; Park et al., 2011). Potential oil yield gains have been identified through molecular studies (Ajjawi et al., 2017; Fukuda et al., 2018; Negi et al., 2020; Park et al., 2019; Prioretti et al., 2020). Nonetheless, cultivation at large scale outdoors is still primarily impeded by algal productivity and other practical considerations. For instance, most operations use batch culture but the process of scaling up from a laboratory culture is prolonged. This could be avoided by operating semicontinuous systems at scale provided careful pathogen control is also exercised (Borowitzka and Vonshak, 2017). Nonetheless, attempts to achieve this have not improved upon batch culture outputs so far, indicating that optimization is still required (Benvenuti et al., 2016; Klok et al., 2014). We focused on semicontinuous culture owing to the potential biotech benefits and more rigorous control of variables at the experimental level.

Thermochemical conversion allows direct production of biofuels from biomass, so in theory, high oil content is not essential for algal biofuel produced in this way, although higher energy inputs are required and there are still some economic caveats to this approach (Mathimani et al., 2018). High oil content is an advantage for physical or chemical extraction methods, particularly relevant for oil for food or feeds. A fundamental problem in biochemical approaches is that the accumulation of oil in algae depends on nutrient depletion or other stresses that compromise growth (Campos et al., 2014; Day et al., 2012; Georgianna and Mayfield, 2012; Huang et al., 2013; Takagi et al., 2006). Under batch culture, algal cells first exhaust

[1]The Scottish Association for Marine Science (SAMS), Scottish Marine Institute, Oban, Argyll PA37 1QA, UK

[2]Advanced Biomanufacturing Centre, Department of Chemical and Biological Engineering, ChELSI Institute, The University of Sheffield, Sheffield S1 3JD, UK

[3]Present address: Marine Research Centre, University of Vigo, 36310 Vigo, Galicia, Spain

[4]Present address: Department of Biosciences, College of Science, Swansea University, Swansea SA2 8PP, UK

[5]These authors contributed equally

[6]Lead contact

*Correspondence: s.vaidyanathan@sheffield.ac.uk

https://doi.org/10.1016/j.isci.2021.102743

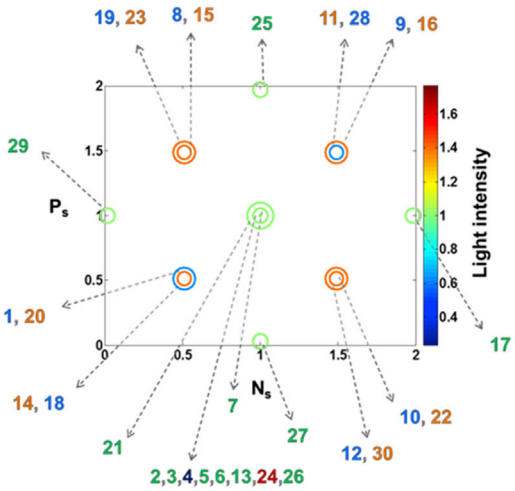

Figure 1. Design space matrix showing 30 core conditions

The conditions for semicontinuous culture are plotted against nitrate (N_s μM) and phosphate (P_s μM) concentration (scale is normalized to the central point which is the median control). Light intensity (μmol m^{-2} s^{-1}) is color coded by the bar; CO_2 (% air) supply is indicated by circle size. Numbers indicate individual runs with colors corresponding to light intensity. The above 4 input data variables are normalized in this diagram to the center point values: controls, which were replicated in 6 runs (#2, 3, 5, 6, 13, 26) (see Table S2 for actual levels). Operational rates are shown in Figures S1A and S1B.

medium nitrogen levels and then with further cell division diminish cellular N content becoming quiescent cells or "liporotunds" which contain large oil droplets (Ngan et al., 2015; Přibyl et al., 2012; Zienkiewicz et al., 2020). It follows that using semicontinuous culture for oil must require a "growth vs. oil induction" trade-off that can be attempted by modifying the conditions. Sufficient knowledge of biological regulation and the environmental "triggers" that drive oil accumulation in microalgae is also desirable for sustainable process developments, as has been widely pointed out (Day et al., 2012; Georgianna and Mayfield, 2012; Greenwell et al., 2010; Mata et al., 2010; Slocombe et al., 2016; Stephens et al., 2010; Wijffels and Barbosa, 2010; Williamsle and Laurens, 2010).

A successful outcome much depends on how a particular algal species responds to these changes. Cell size, in particular, is a master trait in the interaction between nutrient (or light) supply with cell metabolism, ecosystem function, and productivity (Marañón, 2015). In the open ocean, small-celled species dominate in an ecosystem characterized by a constant low-level nutrient supply, whereas in estuarine locations, an intermittent supply at higher concentrations favors larger-celled species (Huete-Ortega et al., 2014; Marañón et al., 2013). Therefore, strain selection must account for inherited traits and niche adaptations such as these (Shurin et al., 2013).

Our aim was to cast light on these regulatory mechanisms, delineating key trends for sustainable oil accumulation without compromising growth. We took a rigorous approach to control variables, using photobioreactor (PBR) arrays under semicontinuous cultivation to optimize culture conditions for oil production (Bi et al., 2014; Bull, 2010; Piepho et al., 2012). Using marine resources can minimize the consumption of freshwater (Day et al., 2012; Mata et al., 2010), so we compared production in 2 unrelated marine strains of different habitats which were preselected for high oil under batch culture. These were a *Nannochloropsis oceanica* strain (CCAP849/10) (oil content and productivity: 53% dry weight [DW] and 13 mg/L/day) where the type strain was oceanic and an estuarine *Chlorella vulgaris* strain (CCAP211/21A) (52% DW and 11 mg/L/day) (Slocombe et al., 2015).

In summary, this multifactorial study was designed to maximize oil content without excessively compromising biomass productivity (BMP). To our knowledge, this study is the first of its kind to use PBR arrays in semicontinuous mode for a comparative analysis of both the physiological and ecology-trait-based fields, for biotechnological performance gains.

RESULTS

Experimental design and overview

To optimize parameters for oil production using response surface methodology (RSM), a matrix of conditions was built with a central composite design. This enabled appropriate coverage of the design space to effectively model the contributing influences with minimal experimental combinations (Figure 1). This was done for cross-species comparison with 4 independent input variables for light, CO_2, stock nitrate (N_s), and

Table 1. Comparison of algal species performance across the experiment

	Conditions #1–31								Center controls (n = 6)					
	N. oceanica			*C. vulgaris*					*N. oceanica*		*C. vulgaris*			
Output parameter	Mean	Min	Max	Mean	Min	Max	Ratio	p value	Mean	RSD (%)	Mean	RSD (%)	Ratio	p value
Growth rate														
μMAX (d^{-1})	0.96	0.27	1.20	0.81	0.26	1.60	1.19	<0.01	1.16	3.70	0.70	17.91	1.65	<0.001
Composition														
TFA (%DW)	24.3	12.9	79.1	17.9	6.5	64.5	1.36	<0.01	16.2	5.4	10.4	27.0	1.56	<0.01
Carbohydrate (%DW)	9.1	6.1	17.6	25.2	6.1	45.4	0.36	<0.001	7.7	8.7	37.8	10.0	0.20	<0.001
Storage (%DW)	33.4	20.1	89.0	43.0	27.1	75.2	0.78	<0.01	23.9	5.2	48.2	9.9	0.50	<0.001
Protein (%DW)	35.3	14.9	50.0	56.4	27.4	82.1	0.63	<0.001	37.6	12.6	63.2	8.0	0.60	<0.001
POP (%DW)	0.57	0.15	0.87	0.33	0.08	0.53	1.71	<0.001	0.71	7.02	0.35	12.76	2.02	<0.001
Chlorophyll (%DW)	0.70	0.11	1.31	1.66	0.20	3.62	0.42	<0.001	0.73	10.72	1.79	21.00	0.41	<0.001
Carotenoid (%DW)	0.61	0.06	1.22	0.50	0.15	1.28	1.20	<0.05	0.65	14.01	0.46	10.44	1.41	<0.01
C/N atomic ratio	12.0	6.5	59.8	12.4	6.6	39.1	0.96	NS	7.7	1.2	9.5	18.1	0.81	<0.05
Concentration														
BMC (mgL^{-1} DW)	263.2	56.3	723.6	458.3	94.0	1366.7	0.57	<0.001	125.1	48.4	389.6	6.2	0.32	<0.001
Medium														
DIN (μM)	1581.7	141.2	4397.8	399.4	0.0	1824.7	3.96	<0.001	1753.6	9.7	32.3	132.7	54.3	<0.001
DIP (μM)	10.56	0.20	51.51	1.84	0.00	20.00	5.74	<0.01	31.91	39.94	0.70	62.98	45.63	<0.01
Productivity														
BMP ($mgL^{-1}d^{-1}$ DW)	78.0	18.5	157.8	79.3	3.8	227.8	0.98	NS	72.7	47.6	116.3	11.9	0.63	<0.05
TFP ($mgL^{-1}d^{-1}$)	17.3	3.6	53.5	11.2	0.9	40.3	1.55	<0.05	11.9	49.6	11.8	16.9	1.01	NS
CH prod. ($mgL^{-1}d^{-1}$)	7.0	1.8	22.3	23.6	0.2	89.7	0.30	<0.001	5.7	57.1	44.6	14.6	0.13	<0.001
Prot. prod. ($mgL^{-1}d^{-1}$)	27.5	3.2	61.1	48.8	1.5	155.2	0.56	<0.001	26.3	36.8	74.1	17.8	0.35	<0.001
Morphology														
Cell diameter (μm)	2.88	2.48	3.61	4.51	3.44	6.81	0.64	<0.001	2.81	2.15	3.85	6.05	0.73	<0.001

Means of all conditions (#1–31) and the center controls (n = 6) were compared. The ratio of mean values from *N. oceanica* as a function of *C. vulgaris* are shown with *p* values indicated (paired 2-tail t test) where significant or not (NS). PBR-PBR variation was assessed by the relative standard deviation (RSD). Storage refers to combined TFA and carbohydrate. BMC = biomass concentration; BMP = biomass productivity; TFP = TFA productivity; CH prod. = carbohydrate productivity; PR Prod. = protein productivity.

phosphate (P_s) concentration, providing a range of input N/P ratios (Table S1, S2). A dilution factor (%μ_{MAX}) was assigned for semicontinuous culture that allowed for the extent of growth limitation (see STAR methods). This dilution factor, along with μ_{MAX}, defined operational rates (ORs) (Figures S1A–S1C). The experiment was carried out in PBR multiarrays (Figures S1D and S1E) initially taking μ_{MAX} data for each condition followed by measurements taken under pseudo steady-state conditions in semicontinuous culture at harvesting end points (Data S1). Nutrient input rates (N_i and P_i) were the product of N_s (or P_s) and the daily replacement volume. The center point controls (Figure 1) allowed cross-species comparison under one set of conditions (n = 6) (Table 1) and determination of PBR-to-PBR variation, enabling an assessment of the repeatability of the experimental setup (Figures S1F and S1G). The multifactorial data were analyzed by a range of methods: cross-species correlation (Figure 2, Table S3, Data S2), 2-dimensional (2D) regression (Figures 2 and 4), RSM (Figure 2), principal component analysis (PCA) (Figure 3), and threshold plots (Figure 5).

Comparison of growth characteristics in the 2 model algae species

Greater maximum salinity tolerance observed in *N. oceanica* compared with *C. vulgaris* was consistent with adaptation toward the respective oceanic and estuarine habitats of the 2 species (Figure S3A). Likewise, light saturation of growth rates was much more evident in *N. oceanica* (at ~200 μmol $m^{-2}s^{-1}$) both for μ_{MAX} readings (batch cultivation) (Figure 2A) and under semicontinuous culture for BMP (Figures 2B and

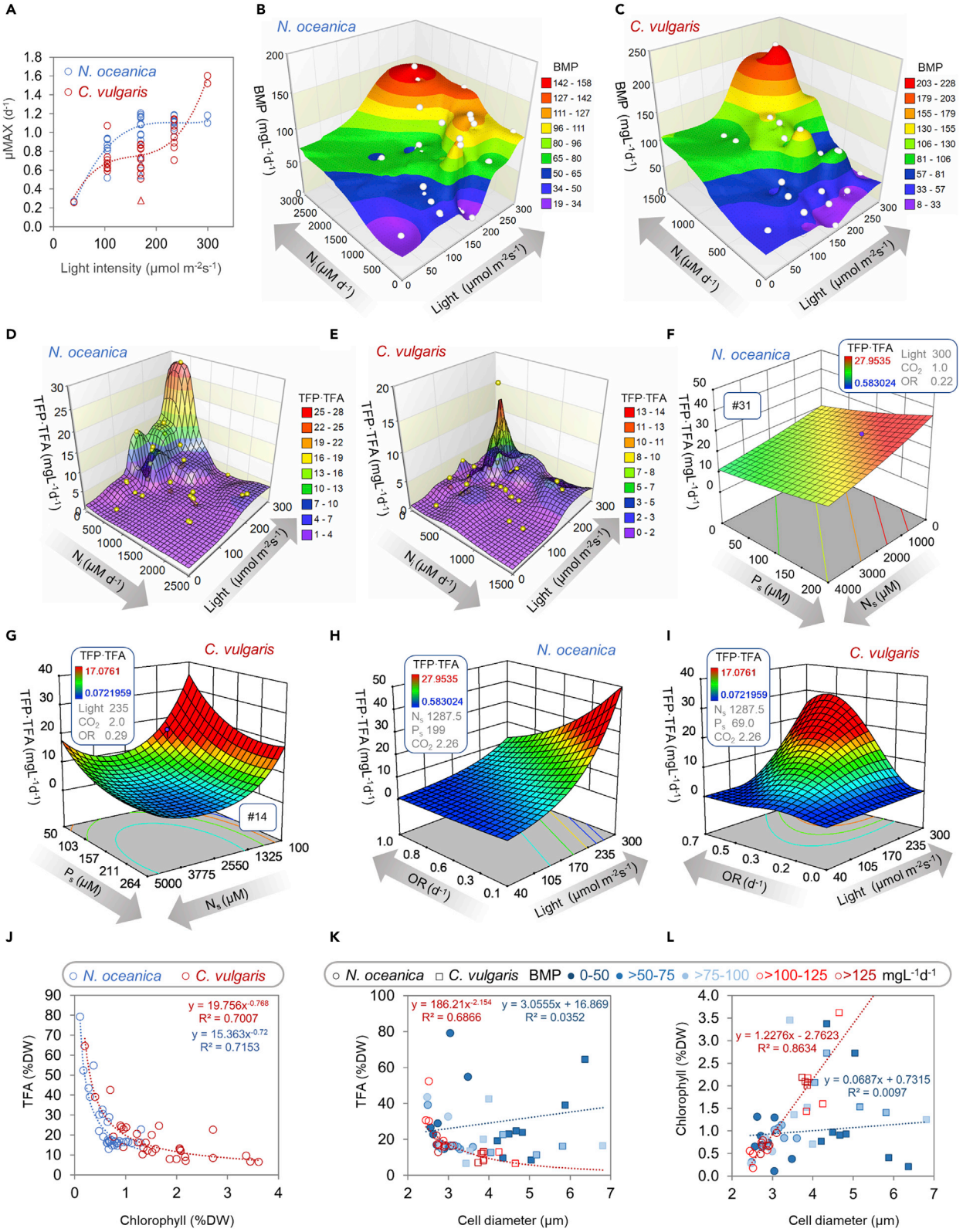
A
μMAX (d-1)
N. oceanica
C. vulgaris
Light intensity (μmol m-2s-1)
B
N. oceanica
BMP (mgL-1d-1)
BMP
142 - 158
127 - 142
111 - 127
96 - 111
80 - 96
65 - 80
50 - 65
34 - 50
19 - 34
N (μM d-1)
Light (μmol m-2s-1)
C
C. vulgaris
BMP (mgL-1d-1)
BMP
203 - 228
179 - 203
155 - 179
130 - 155
106 - 130
81 - 106
57 - 81
33 - 57
8 - 33
N (μM d-1)
Light (μmol m-2s-1)
D
N. oceanica
TFP·TFA (mgL-1d-1)
TFP·TFA
25 - 28
22 - 25
19 - 22
16 - 19
13 - 16
10 - 13
7 - 10
4 - 7
1 - 4
N (μM d-1)
Light (μmol m-2s-1)
E
C. vulgaris
TFP·TFA (mgL-1d-1)
TFP·TFA
13 - 14
11 - 13
10 - 11
8 - 10
7 - 8
5 - 7
3 - 5
2 - 3
0 - 2
N (μM d-1)
Light (μmol m-2s-1)
F
N. oceanica
TFP·TFA (mgL-1d-1)
TFP·TFA
27.9535
0.583024
Light 300
CO2 1.0
OR 0.22
#31
Ps (μM)
Ns (μM)
G
C. vulgaris
TFP·TFA (mgL-1d-1)
TFP·TFA
17.0761
0.0721959
Light 235
CO2 2.0
OR 0.29
#14
Ps (μM)
Ns (μM)
H
N. oceanica
TFP·TFA (mgL-1d-1)
TFP·TFA
27.9535
0.583024
Ns 1287.5
Ps 199
CO2 2.26
OR (d-1)
Light (μmol m-2s-1)
I
C. vulgaris
TFP·TFA (mgL-1d-1)
TFP·TFA
17.0761
0.0721959
Ns 1287.5
Ps 69.0
CO2 2.26
OR (d-1)
Light (μmol m-2s-1)
J
N. oceanica
C. vulgaris
y = 19.756x-0.768
R² = 0.7007
y = 15.363x-0.72
R² = 0.7153
TFA (%DW)
Chlorophyll (%DW)
K
N. oceanica
C. vulgaris
BMP
0-50
>50-75
>75-100
>100-125
>125
mgL-1d-1
y = 186.21x-2.154
R² = 0.6866
y = 3.0555x + 16.869
R² = 0.0352
TFA (%DW)
Cell diameter (μm)
L
y = 1.2276x - 2.7623
R² = 0.8634
y = 0.0687x + 0.7315
R² = 0.0097
Chlorophyll (%DW)
Cell diameter (μm)

Figure 2. Maximization of oil productivity and content

(A) Cross-species analysis of maximum growth rate (μ_{MAX}) showing light-saturation curves for multivariate conditions under batch culture. Conditions which were not light-limited (Δ) were excluded from curve fitting (these were identified in Figure S2).

(B and C) Growth of the 2 algae under semicontinuous conditions indicated by surface plots of BMP in relation to light and N supply (N_i).

(D and E) Optimal oil content and productivity indicated by the TFP·TFA product in relation to light and N supply (N_i) in semicontinuous culture.

(F–I) Modeling to optimize TFP·TFA by RSM in relation to the N and P concentration supplied (F and G) and in relation to operational rate (OR) vs. light (H and I). In (F and G), the parameters were used from the best experimental conditions found for TFP·TFA (F, #31; G, #14) and these are shown inset and with pins (●). In (H and I), the parameters were preoptimized (within design-space) values using the model (inset). (J–L) Cross-species relationships in semicontinuous culture showing (J) TFA and chl content; cell diameter with TFA content (K) and chl (L). In (K and L), the BMP achieved for each data point is indicated by color-coding and best fit curves were produced for high BMP (…) >100 mg L^{-1} day^{-1} and low BMP (…) <50 mg L^{-1} day^{-1}. Data points from semicontinuous culture were means of end point values taken on 3 consecutive days (n = 3).

2C). With *C. vulgaris*, maximum growth rates were higher in both modes of cultivation (μ_{MAX} 1.60 cf. 1.20 d^{-1} and BMP 230 cf. 160 $mgL^{-1}d^{-1}$) (Table 1). Therefore, overall, this estuarine strain appeared to be better adapted for growth at high light, as expected in this benthic environment. Furthermore, there was evidence for poorer growth of this species under lower light. The dip in *C. vulgaris* μ_{MAX} among the center controls at 170 μmol $m^{-2}s^{-1}$, relative to *N. oceanica*, was significant (t test: n = 6, $p < 0.001$) (Figure 2A; Table 1). When other data points at this particular light intensity were examined, inhibition of *C. vulgaris* μ_{MAX} was found at high nitrate (5 mM) along with a lack of N/P/C-limitation at the lowest inputs (50 μM N, 4 μM P or air) (Figure S2). These observations were consistent with the lesser growth seen in the center controls in this species (Figure 2A). In contrast, *N. oceanica* did show N/P/C-limitation at these 3 low extremes but no indication of nitrate inhibition, consistent with the higher growth rate of center controls at 170 μmol $m^{-2}s^{-1}$ (Figure S2).

There were also species-specific differences in the way growth responded across the matrix of semicontinuous culture conditions. In *N. oceanica*, growth appeared to be mostly colimited by light and N supply (N_i), whereas in *C. vulgaris*, growth was more limited by N supply criteria. This was indicated by regression analysis (R^2) and Pearson correlation coefficients (r_p) shown in Table S3 and Data S2, as follows. With *N. oceanica*, the growth proxy BMP showed most dependency on light (R^2 0.37 and r_p 0.6: $p < 0.001$) and N_i (N supply rate) (R^2 0.22; r_p 0.4: $p < 0.02$), higher than the other nutrient supply factors (N_i, P_i, CO_2) and OR. In contrast, with *C. vulgaris*, the overall dependency of BMP across the experiment on light was low (R^2 0.07; r_p 0.2: NS) but was primarily dependent on N_i (R^2 0.72; r_p 0.9: $p < 0.001$). Similar trends were seen with 2D surface regression plots showing BMP in relation to the 2 key factors, light and N_i (Figure 2). Here, a symmetrical surface plot with *N. oceanica* supported an equal influence on variance (Figure 2B) compared with *C. vulgaris*, where a greater influence of N_i over light was evident – the influence of the light in this species was somewhat localized (Figure 2C). The greater influence of N supply over P supply for growth (seen in regression data, above) was mirrored in surface plots of BMP. In both algae, greater BMP was seen with a high N/P input ratio (above Redfield) than with low N/P (Figures S7A and S7D).

Taken together, species-dependent differences in the rate of growth, such as adaptation to high light or salinity were identified and these could be related to the ecological niche. Variation in the dependency of growth on light and N supply in the 2 species was explored further in terms of oil production (below). Despite these different growth characteristics, it was found that the mean growth rate proxies across the experiment were similar for the 2 species: μ_{MAX} (0.81–0.96 d^{-1}) (batch culture) and BMP (~80 $mgL^{-1}d^{-1}$) (under semicontinuous culture) (Table 1). Therefore, it was considered meaningful to compare the 2 species further.

Differences in oil productivity under semicontinuous growth

To gain an overview of resource partitioning into storage products, the mean performance of the 2 species was examined. In Table 1 (and Figures S1F and S1G) comparisons were made using (i) the median control data (n = 6) and (ii) the full multivariate data set. Except for end point dissolved inorganic nitrogen (DIN) and dissolved inorganic phosphate (DIP), comparison of the 2 species with either data set gave similar outcomes. In *N. oceanica*, proxies for mean oil content and productivity (TFA [total fatty acids] and TFP [TFA productivity]) were 1.4–1.6 times higher ($p < 0.05$). Conversely, those for carbohydrate (CH) were 3 times higher in *C. vulgaris* ($p < 0.001$). In fact, carbohydrate (CH) content was never more than 18% DW in *N. oceanica*. The preference for oil accumulation in *N. oceanica* was seen despite evidence for less nutrient stress than *C. vulgaris* (mean end point DIN and DIP levels were 4–6 times higher over all conditions; 50 times higher in center controls in *N. oceanica*) and less nutrient demand (suggested by 2–3 times lower mean end point biomass concentrations [BMCs] in *N. oceanica*) (Table 1).

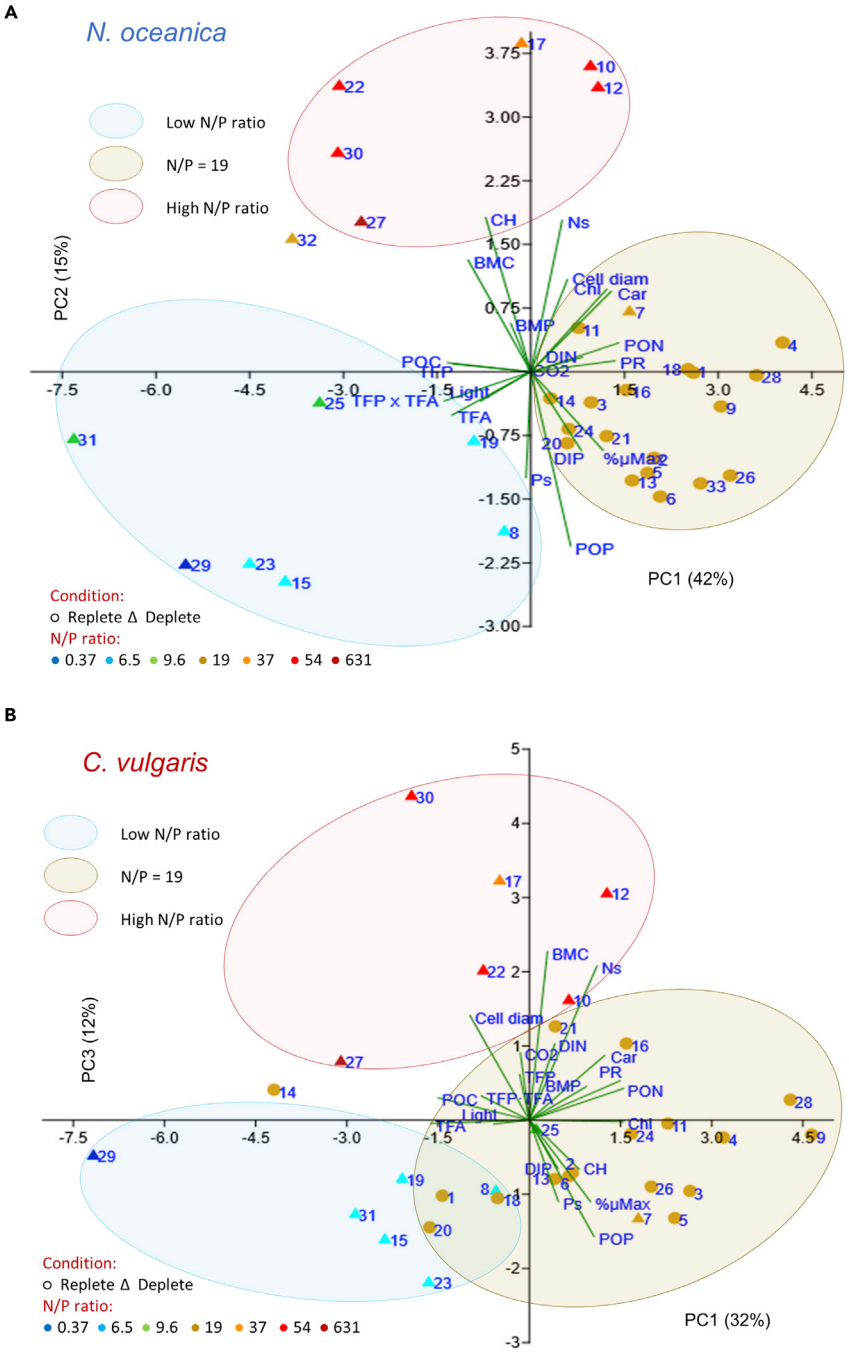

Figure 3. Effect of growth conditions on biomass traits and morphology

Correlation matrix PCAs are shown for *N. oceanica* (A) and *C. vulgaris* (B) for mean end point data (n = 3) under semicontinuous culture. The 5 independent input factors were light, CO_2, N_s, P_s, and $\%\mu_{MAX}$. Also shown are oil content proxies (TFA, POC); photosynthetic proxies (protein [PR], carbohydrate [CH], PON, chlorophyll [chl], carotenoids [car]); culture medium end points: DIN and DIP; oil productivity proxies (TFP, TFP·TFA); biomass concentration (BMC), biomass productivity (BMP) and cell diameter. The inter-relationships and importance of these factors are indicated by biplot (–) orientation and length. The N/P ratio values and the specific conditions are indicated by symbol shape, color and encompassing ovals (inset). The panels showing best data separation are depicted here. The full set of panels is shown in Figure S4 for PC1-3 along with principal component % variance (shown here on axes). Bootstrap N = 100.

To summarize, *N. oceanica* had better oil productivity than *C. vulgaris* across the matrix of semicontinuous culture conditions but showed light saturation leading to poorer maximum growth (i.e. BMP). *N. oceanica* was more predisposed to oil production despite experiencing less nutrient demand, depletion, or limitation.

Modeling for optimization of high oil content and oil productivity

For algal oil production, it would be beneficial to strike a trade-off between high oil content (for ease of extraction) and oil productivity (TFP). Therefore, the product: TFP·TFA was chosen as a practical factor for optimization in models. This factor is also biologically meaningful because natural selection often operates through product-content and product-specific output parameters combined. For instance, in the case of arboreal flowers, nectar content and floral quantity are both significant for attracting insect pollinators (Brito et al., 2015; Wetherwax, 1986).

Modeling TFP·TFA response to growth conditions with RSM equations indicated the prime role of the incident light, followed by N_s or OR (Figure S3B). In surface plots with these factors, a limited region of low N_i (a function of N_s and OR) and high light was defined that magnified TFP·TFA (Figures 2D and 2E). The TFP·TFA peak was better supported in *N. oceanica* but lay at the corner of the design space, suggesting better production with further N-supply restrictions and higher light was possible.

The conditions for maximum TFP·TFA were #31 (*N. oceanica*) and #14 (*C. vulgaris*) with growth parameters and RSM plots as shown (Figures 2F and 2G). In *N. oceanica*, the experimental maximum TFP of 54 $mgL^{-1}d^{-1}$ with 52% DW TFA was achieved in condition #31 and in *C. vulgaris*, a maximum TFP of 40 $mgL^{-1}d^{-1}$ with 42% DW TFA was achieved in condition #14 (Table 1) (Data S1). Therefore, better results for oil production were obtained with *N. oceanica*.

The conditions that elicited maximum oil production in the 2 species were different suggesting different responses toward stress. Comparison of the 2 maxima indicated a bias toward N-stress imposition in *N. oceanica* #31 and toward synergistic imposition of N- and P-stress in *C. vulgaris* #14. This was seen in the nutrient-/light-supply ratios such that N_i/L in *N. oceanica* #31 was lower (0.8 cf. 1.37), whereas P_i/L was lower in *C. vulgaris* #14 (0.073 cf. 0.088). The N/P input ratio for condition #31 was also low (9.6), whereas #14 was at around the Redfield ratio (19) (Data S1).

End point data at these maximal conditions suggested equal P stress but paradoxically less N stress received in *N. oceanica*. So, in both cases, there was near-complete P assimilation (end point DIP 0.66 cf. 1.6 μM) and low biomass P levels (end point particulate organic phosphorus [POP] 0.27 cf. 0.22 %DW) (Data S1). Whereas, in *N. oceanica* #31, N-assimilation appeared to be incomplete since end point DIN levels were much higher than in *C. vulgaris* (DIN 703 cf. 4.1 μM) (Data S1). This suggested that *N. oceanica* had a lower threshold for perception and mitigation of N-stress and this was explored further.

The modeling (RSM analysis) also indicated that low N/P input ratio favored high TFP·TFA in *N. oceanica* (Figure 2F), whereas low levels of both N and P supply (near-Redfield ratio) were required in *C. vulgaris*, suggesting synergism (Figure 2G). Low OR in *N. oceanica* was a positive influence (Figure 2H), whereas in *C. vulgaris*, a relatively high OR was required, and here, a design space optimum was achieved (Figure 2I). Similar modeling of carbohydrate (CH) production (CHP·CH) was linked to a high N/P ratio in *N. oceanica* and replete conditions in *C. vulgaris* (Figure S3).

In summary, data modeling using inputs (conditions) indicated better co-optimization of oil content and oil productivity (TFP·TFA) in *N. oceanica*. This was achieved by low input N/P ratio and low OR, whereas a high N/P ratio favored CH. This differed from *C. vulgaris* where synergistic NP depletion for oil was required and CH associated instead with repletion. Modeling of oil production based on input data parameters indicated differences in regulation that were explored further using multivariate analyses.

The interplay of nutrient regulation and cell size influences oil productivity

PCA analysis provided a holistic interpretation, identifying 3 key influences common to both algae and highlighting some interesting differences (Figures 3 and S4). More than 60% of variance was explained by principal components 1–3 (Figure S4). In Figure 3, the most effective data separations are shown with PC1 vs. PC2 or PC3, for the 2 algal species, with the full set of graphs shown in Figure S4.

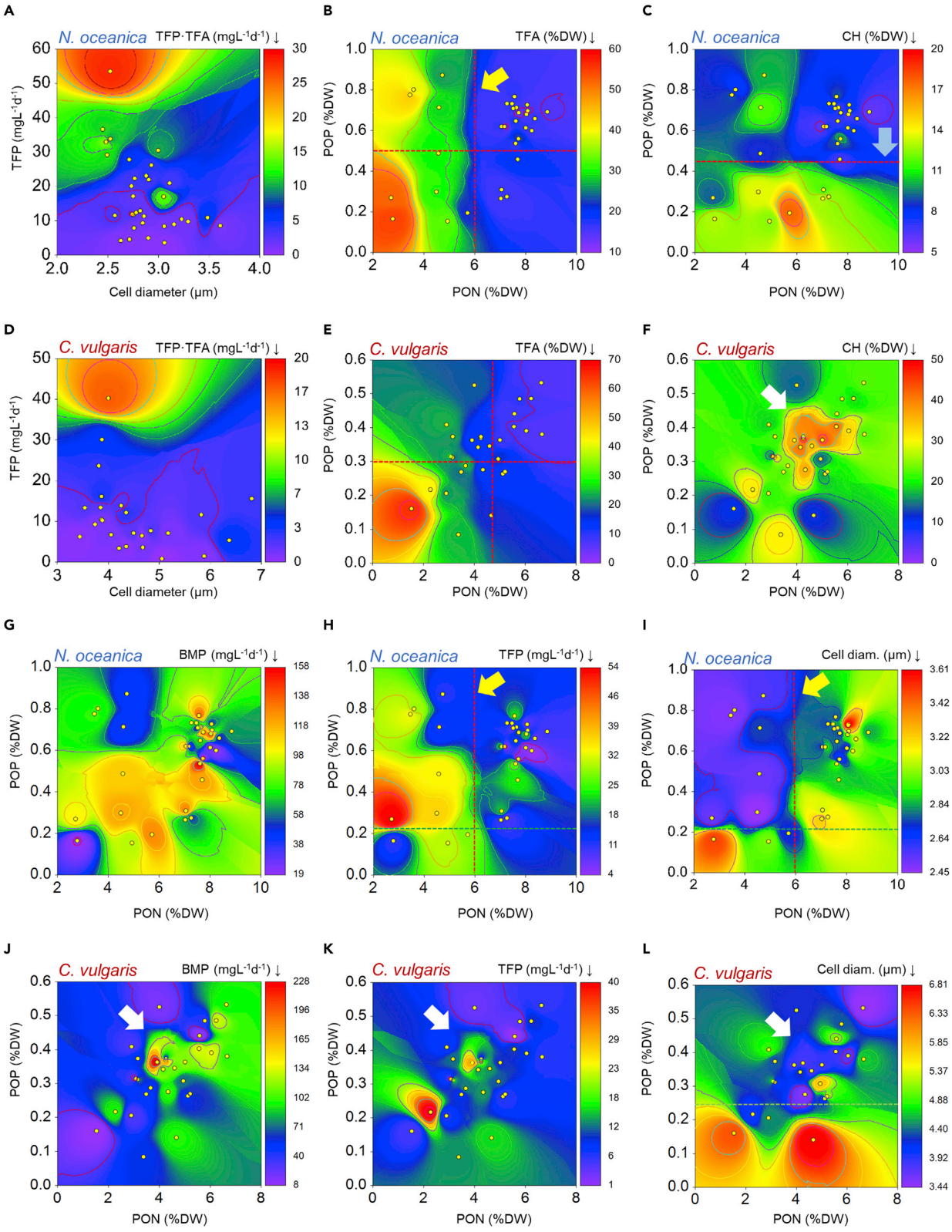
A
N. oceanica TFP·TFA (mgL-1d-1) ↓
TFP (mgL-1d-1)
Cell diameter (μm)
B
N. oceanica TFA (%DW) ↓
POP (%DW)
PON (%DW)
C
N. oceanica CH (%DW) ↓
POP (%DW)
PON (%DW)
D
C. vulgaris TFP·TFA (mgL-1d-1) ↓
TFP (mgL-1d-1)
Cell diameter (μm)
E
C. vulgaris TFA (%DW) ↓
POP (%DW)
PON (%DW)
F
C. vulgaris CH (%DW) ↓
POP (%DW)
PON (%DW)
G
N. oceanica BMP (mgL-1d-1) ↓
POP (%DW)
PON (%DW)
H
N. oceanica TFP (mgL-1d-1) ↓
POP (%DW)
PON (%DW)
I
N. oceanica Cell diam. (μm) ↓
POP (%DW)
PON (%DW)
J
C. vulgaris BMP (mgL-1d-1) ↓
POP (%DW)
PON (%DW)
K
C. vulgaris TFP (mgL-1d-1) ↓
POP (%DW)
PON (%DW)
L
C. vulgaris Cell diam. (μm) ↓
POP (%DW)
PON (%DW)

Figure 4. Nutrient status and cell diameter in relation to productivity

Contour plots are shown for the 2 algae species in alternating rows. In (A and D) the relationship between TFP·TFA, TFP and cell diameter is shown. The remainder of the panel shows the relationship of biomass nutrient status (end point PON and POP) in respect to TFA content (B and E); carbohydrate (CH) content (C and F); biomass productivity (BMP) (G and J); oil productivity (TFP) (H and K), and cell diameter (I and L). Individual data points (●) are replicate culture conditions (n = 3). Estimated from the contour boundaries are lines (—) referring to stress-induction thresholds (for products or small cell sizes) and lines (—) referring to large cell size induction. Colocalization in *N. oceanica* of high TFA content, high TFP, and small cell size is indicated (→). Induction of carbohydrate (CH) in *N. oceanica* is also shown (→). Colocalization in *C. vulgaris* of high CH content, high BMP, and small cell size is highlighted (→).

The 3 key influences common to the 2 species were (i) the opposition of oil content proxies (TFA, particulate organic carbon [POC]) and light vs. photosynthetic investment proxies (protein [PR], chlorophyll [chl], carotenoids) – of prime importance due to association with PC1 (>30% variance explained, Figure S4); (ii) input N/P ratio – data separation along y axes in Figure 3; and (iii) opposition of growth (BMP) and oil productivity (TFP) vs. cell diameter – along y axes in Figures S4B and S4D. The first key influence was anticipated, given that chl levels have long been used as an inverse proxy for oil (TFA content) (Figure 2J).

Concerning the second key factor: input N/P ratio, a clear 3-way separation of data was noted according to low or high N/P ratio and nutrient repletion (Figure 3). Oil content (TFA) in both algae was favored most by low N/P input ratio, but a high N/P ratio was also influential (Figures 3 and S4). This observation was supported by regression analysis (both algae) of oil proxies (TFA, POC, C/N, particulate organic nitrogen [PON], PR, chl) where variance was chiefly explained by N-supply input factors (N_i, N_s or log N/P input) (R^2 0.5–0.8) (Table S3, Data S2). Steady-state (end point) BMC was associated with a high N/P input ratio in both species (Figures 3 and S4) and confirmed with surface plots (Figures S5A and S5B). This bias was also noted with growth rate (BMP) (Figures S7A and S7D).

PCA analysis also highlighted important differences between the 2 algal species. In *N. oceanica*, end point DIN more clearly opposed TFA, indicating a strong influence for N depletion despite DIN levels being very high compared with *C. vulgaris* (Figures 3 and S4) (Table 1). This led to the concept of differing stress thresholds (below).

Another major difference between the species was in the regulation of carbohydrate levels. Increases were linked to P deficiency in *N. oceanica*, shown by its association with high N/P ratio and opposition to markers of P sufficiency or repletion (DIP, POP, P_s, $\%\mu_{MAX}$) (Figure 3). In contrast, with *C. vulgaris*, carbohydrate levels associated with P-sufficiency markers, better growth (see BMP biplot) or replete conditions, and clearly opposed cell diameter (Figures 3 and S4).

In *N. oceanica*, a closer association was seen of the TFA and TFP biplot vectors with the low N/P ratio data point cluster (PC1 vs. PC2, less so in PC1 vs. PC3), indicating a lesser trade-off penalty of oil content versus oil productivity compared with *C. vulgaris* (divergent in both PC1 vs. PC2/3) (Figures 3 and S4).

Concerning the opposing (inverse) relationship of cell size and productivities revealed by PCA (Figure S4), cell diameter opposed TFP more than BMP in *N. oceanica* and vice versa in *C. vulgaris* (Figures S4B and S4D). This bias of small cell size toward high oil productivity (TFP) was also visible in data regression plots, and the trend was clearer in *N. oceanica* (Figures 4A and 4D) (r_p −0.48: $p < 0.005$ cf. −0.28 NS; Data S2). In *C. vulgaris*, small cell size associated better with high carbohydrate productivity (CHP) than in *N. oceanica* (Figures S5C and S5D) (r_p −0.56: $p < 0.004$ cf. −0.21 NS; Data S2).

The combined effect of N and P status on biomass composition and productivity was explored further in 2D regression contour plots for end point PON and POP (Figure 4). The data sets in Figures S6 and S7 also compare end point DIN and DIP and nutrient supply rates (N_i, P_i). These 3 independent proxies for nutrient status showed similar results. In both species, high PR content localized to the nutrient-replete regions (Figure S6). With *N. oceanica*, there was a clear demarcation of the high TFA and carbohydrate content into respectively low-N (Figure 4B) and low-P zones (Figure 4C; Figure S6). Within the low-N zones, there was a bias toward small cell size and high oil productivity (TFP) (Figures 4I cf. 4B and 4H; Figures S6 and S7).

With *C. vulgaris*, high TFA content was also located to the low-N zone but pointed toward a more synergistic NP-stress response (Figures 4E cf. 4B; Figure S6). High carbohydrate content in this alga consistently occupied a central zone in the NP contour plots suggesting that it was both an intermediate-stress product and synergistically regulated (Figures 4F and S6). This central zone of high carbohydrate also corresponded

to small cell size (Figures 4F cf. 4L) and high growth rate (BMP) (Figures 4F cf. 4J; Figure S6). In *C. vulgaris*, large cell size was largely confined to the low P-supply/P-status zones (Figures 4L, S6, and S7).

In summary, multivariate analyses linked high TFA content and oil productivity (TFP) in *N. oceanica* to small cell size and low N/P ratio. In contrast, both carbohydrate and TFA induction required synergy of N and P stress in *C. vulgaris*. In this species, carbohydrate was preferentially induced as an intermediate-stress product and levels were closely linked to small cell size. P stress was associated with larger cells, particularly in *C. vulgaris*.

Model for small cell size and oil productivity

The evident bias toward oil accumulation in *N. oceanica* was examined next, considering factors such as cell size regulation and the large investment of C made in photosynthesis, indicated by chl content. chl content was found to be a good cross-species inverse proxy for TFA content (Figure 2J). Although greater chl levels were observed in *C. vulgaris*, these data points were found mostly in cases where TFA content had dropped below the 16% DW level which in *N. oceanica* was the baseline for TFA (Figure 2J). Therefore, it appeared that *N. oceanica* was able to constrain investment of C into photosynthesis, in favor of maintaining a minimum TFA level, unlike *C. vulgaris*. This suggested a preference for oil accumulation over photosynthetic capacity in *N. oceanica* but the question was how could this translate into higher oil production?

Morphologically, both species were small-celled, near-spherical alga, but *N. oceanica* was the smallest, and there was only a slight overlap in the cell diameter ranges (2.5–3.6 μm cf. 3.4–6.8) (Table 1). *C. vulgaris* had a propensity to form multicell clusters, which was absent in *N. oceanica*. Interestingly, for those conditions achieving high growth (i.e. BMP>100 $mgL^{-1}d^{-1}$ which was equivalent to the >70th percentile for both species: Data S1), oil content (TFA) showed an inverse cross-species correlation (R^2 0.7) with cell size (Figure 2K). This subset also showed a linear relationship of chl content with cell size (R^2 0.9) (Figure 2L). Low growth conditions (BMP<100 $mgL^{-1}d^{-1}$) showed no correlation of cell size to TFA or chl content (Figures 2K and 2L). There was a similar cross-species correlation with PR, but with carbohydrate, no contiguity between species was seen (Figures S5E–S5G). Because (i) the positive correlation of cell size and chl content and (ii) the negative correlation of cell size and TFA content were only seen for high growth conditions, it was inferred that high oil productivity (specifically high oil content combined with good growth) required small cells to allow better light absorption. The correlations suggested that a higher surface area/volume ratio associated with reduced cell size could counteract the reduced photosynthetic capacity that was associated with elevated oil, permitting good growth.

Although it is generally understood that small cell size favors greater growth rates (e.g. for the BMP proxy here), this factor alone was seemingly insufficient to account for the association of small cell size with greater oil productivity (TFP) in *N. oceanica*. Here, there was a much better inverse correlation of cell size with TFP (r_p −0.48: $p < 0.005$) than with BMP (r_p −0.26: NS) (Data S2). There was also a close association of small cell size, low N status (low PON, DIN, N_i) and high TFP but not with high BMP in surface plots for *N. oceanica* (Figures 4G–4I; Figures S7A–S7C and S7G–S7I). This disparity was consistent with cell size being downregulated to favor a switch of C partitioning from photosynthesis to oil because that would not be expected to favor an actual increase in BMP. Instead, this should lead to the poorer inverse correlation for BMP with cell size in this experiment than seen with TFP.

In *C. vulgaris*, there was a close inverse correlation with cell size to carbohydrate productivity (CHP) (r_p −0.56: $p < 0.004$) and with BMP (r_p −0.48: $p < 0.01$) but not so for TFP (r_p −0.28: NS) (Data S2). In surface plots based on nutrient status, central regions are evident of high CH content, small cell size, and high BMP (less so for TFP) (Figures 4F cf. 4J to 4L; S6 and S7). As seen with both species, there was no evidence that C for CH might be partitioned away from photosynthetic investment (above), even though cell size correlates inversely with CH levels quite well (r_p −0.71: $p < 0.001$) (Data S2).

Relevant to how cell size might be regulated, in *N. oceanica*, small cell size (and high TFP) appeared to associate with a combination of low N status (e.g. PON<6%DW) with sufficient P status (e.g. POP>0.2% DW) (Figure 4I). This bore similarity to the low N/P input ratio conditions that favored oil accumulation along with small cell size and high TFP (Figures S6, S7B and S7C). In *C. vulgaris*, the peak TFP condition appeared to require a combination of low N and P status (at near-Redfield N/P supply ratio) and this associated with small cell size as well as oil accumulation (Figures 4E, 4K, 4L, S7E and S7F). Here, small cell size is confined to a central region in surface plots of PON vs. POP (Figure 4L) or Ni vs. Pi (Figure S7F).

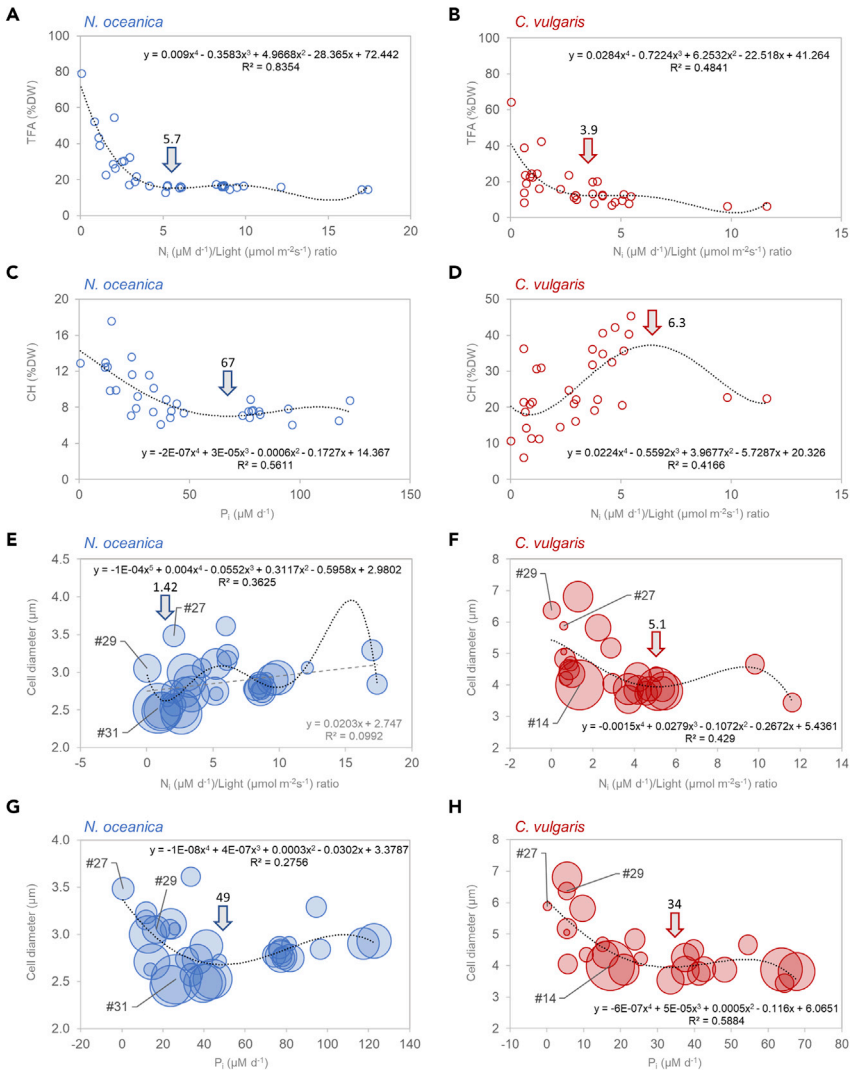

Figure 5. Starvation-threshold responses

Threshold responses are shown for *N. oceanica* (left) and *C. vulgaris* (right). Optimal threshold responses are displayed here based on the most variance explained (R^2). The full data sets are found in Figure S8 for balance. In (A and B), TFA accumulation, and in (C and D), carbohydrate (CH) accumulation is presented in relation to diminishing N supply/light ratio (N_i/L) or P supply (P_i). In (E–H) Cell diameter changes are depicted in relation to N-supply/light ratio (N_i/L) (E and F) and P-supply (P_i) (G and H), where bubble diameter refers to TFP (relative scale). Threshold break points are shown with vertical arrows and the x axis value. Threshold break points were estimated from turning points of curve-fitting polynomials (shown). R^2 indicated closeness of fit and provided a measure of turning point validation. Best oil productivity (TFP) conditions for each species are shown: #31 *N. oceanica* or #14 *C. vulgaris*, along with the nutrient-stress extremes: #29 (N-stress); #27 (P-stress).

To summarize, *N. oceanica* had better oil productivity than *C. vulgaris* across the matrix of semicontinuous culture conditions. One reason could be a preferential C partitioning into oil combined with maintenance of small cell size. The latter appeared to favor good growth with less photosynthetic capacity available. This occurred despite the former species experiencing less nutrient demand, depletion, or limitation. The reason for this was investigated next.

Oil productivity also depends on low starvation thresholds

Despite the multivariate nature of the data, certain growth condition input parameters appeared to play a key role for certain outputs or physiological responses, as described above. This allowed univariate

Table 2. Estimates of potential thresholds for induction of storage components and cell size regulation

		Input factor			Endpoint concentration			
		N_i/Light	N_i	P_i	DIN	DIP	PON	POP
Category	Change	(μMd^{-1})/($\mu molm^{-2}s^{-1}$)	(μMd^{-1})	(μMd^{-1})	(μM)	(μM)	(%DW)	(%DW)
N. oceanica								
TFA (%DW)	↑	5.7	859	39	1306	42.8	7.8	0.61
	↑[a]	ND	600	26	1000	1.5	6.0	0.50
	Mean	5.7	730	33	1153	22	6.9	0.6
Carbohydrate (%DW)	↑	11.3	1953	67	2770	13.8	9.1	0.63
	↑[a]	ND	Δ	40	1000	1.5	6.4	0.45
	Mean	11.3	1953	54	1885	7.6	7.8	0.5
Cell diameter (μm)	↓	7.1	932	108	3030	49.0	8.3	0.68
	↓[a]	ND	550	90	950	Δ	6.0	0.68
	Mean	7.1	741	99	1990	49	7.2	0.7
	↑	1.4	197	49	482	26.0	4.6	0.42
	↑[a]	ND	200	49	400	3.2	3.8	0.22
	Mean	1.4	199	49	441	14.6	4.2	0.3
C. vulgaris								
TFA (%DW)	↑	3.9	334	16	933	5.3	5.7	0.39
	↑[a]	ND	500	8	200	0.1	4.8	0.30
	Mean	3.9	417	12	567	2.7	5.3	0.3
Carbohydrate (%DW)	↑	11.5	1051	54	434	8.4	6.7	0.53
	↑[a]	ND	1000	55	400	8.0	6.3	0.46
	Mean	11.5	1025	54	417	8.2	6.5	0.5
	↓	6.3	751	40	Δ	2.4	4.1	0.36
Cell diameter (μm)	↓	9.3	Δ	54	448	8.4	4.8	0.41
	↓[a]	ND	1000	54	100	5.0	6.5	0.44
	Mean	9.3	1075	54	274	6.7	5.7	0.4
	↑	5.1	1149	34	Δ	2.6	3.2	0.30
	↑[a]	ND	450	22	4	0.1	2.8	0.25
	Mean	5.1	800	28	4	1.3	3.0	0.3

Threshold breakpoints were calculated from univariate plots shown in Figure 5 and Figures S8–S12 or alternatively, where indicated,[a] estimated from bivariate heatmap contour lines (Figures 4 and S6). These two values were averaged (mean). N.D. data not determined and (Δ) threshold not present. Arrows indicate the direction of change.

relationships to be discerned. However, high-order polynomials were required to adequately fit the data, owing to multifactorial influences even in these apparent univariate relationships (Figure S14). Nevertheless, we employed these relationships primarily to interpret indicative threshold breakpoints and not as a predictive tool. It was found that plots of storage product levels or cell size against specific nutrient supply or status parameters often revealed threshold-type responses toward diminishing nutrient levels. These typically showed a transition (break point) from no input-parameter effect at all, under presumed repletion conditions, to one of close correlation (Figures 5 and S8–S12). Defining and comparing the break points between the species revealed differences in stress regulation responses. Specifically, a higher break point value indicated a lower threshold for a stress response (Table 2).

Threshold responses of TFA and CH content in response to nutrient supply rates are shown in Figures 5A–5D (full data set in Figure S8). Similar trends were seen for nutrient status: DIN, DIP (Figures S9) and PON, POP (Figure S10). In both species, the N supply/light ratio (N_i/L) correlated well with TFA induction, better than N_i or P_i alone (Figures 5A and 5B cf. S8A–S8F). This was also seen with *C. vulgaris* carbohydrate induction (Figures 5D cf. S8J–S8L). With carbohydrate content in *N. oceanica*, the most variance was explained

instead by the P supply factors (P_i and e.g. OR, $\%\mu_{MAX}$: R^2 0.5–0.6 Table S3). This resulted in a clearer induction threshold response with P_i indicated by R^2 and a more meaningful estimate of the break point (Figure 5C cf. N_i/L or N_i in Figures S8G–S8I).

Threshold break points are listed in Table 2 and are also depicted on contour plots in Figures 4 and S6. These data show higher break points (lower stress thresholds) for TFA induction in *N. oceanica* compared with *C. vulgaris*. For N-stress, 1.5–3 times higher (N_i/L, Figures 5A and 5B) (N_i, Figures S8B and S8E) (DIN, Figures S9A and S9C) (PON, Figures S10A and S10C) and 2–8 times higher with P stress (P_i, Figures S8C and S8F) (DIP, POP: Figures S9B and S9D; S10B and S10D) (Table 2). Interestingly, carbohydrate induction break points in *C. vulgaris* were in turn 2–3 times higher than for TFA (with N_i/L, N_i, P_i, and DIP) (Figures 5D cf. 5B, S8J–S8L cf. S8D–S8F, S9H cf. S9D). Together, this observation and the unimodal responses (to N_i/L, N_i, P_i, DIP) (Figures 5D and S8J–S8L, and S9H) suggested that carbohydrate was an intermediate-stress product, in agreement with the multivariate analysis (above).

To summarize, lower stress thresholds (i.e. higher break points) were evident for oil induction in *N. oceanica*, apparently prioritizing its accumulation. Lower thresholds were instead seen for carbohydrate in *C. vulgaris*, consistent with it being an intermediate C-storage product before oil accumulation.

High stress thresholds for cell size could improve oil productivity

The link between high oil productivity and cell size (negative correlation, above) was explored further in terms of nutrient-stress thresholds (Table 2; Figures 4I, 4L, 5E–5H, S8, S11 and S12) and variance explained (Table S3). In Figure 5, nutrient supply vs. cell diameter plots are shown with bubbles to indicate TFP levels.

In both algae, phosphate (alone or in combination with light) accounted for much cell size variance – more than nitrate. For *N. oceanica*: $P_s \cdot L$ (R^2 0.5) (Figures S11A and S11C), P_s (R^2 0.35) cf. light (R^2 0.2), N_s or CO_2 (R^2 0.1), and for *C. vulgaris*: P_i/L (R^2 0.7) (Figure S11B and S11D); $\%\mu_{MAX}$ (R^2 0.7), P_i (R^2 0.5) cf. N_i (R^2 0.4), light, or CO_2 ($R^2 < 0.1$) (Table S3).

Also in both species, diminishing P supply was linked to a threshold-type upturn in cell size within the middle of the experimental range for P supply (Figures 5G and 5H). The turning points for cell size increase and CH induction with P stress also coincided in *N. oceanica* (P_i = 49 cf. 67 $\mu M\ d^{-1}$) (Figures 5G cf. 5C) (Table 2). In *N. oceanica*, there was first a downwards trend with decreasing P supply (Figure 5G) and to a limited extent, P status (DIP: Figure S12C and POP: Figure S12G). This initial downwards trend was only seen with DIP for *C. vulgaris* (Figure S12D) being absent with P-supply (P_i) or POP (Figures 5H and S12H).

With diminishing N supply, *C. vulgaris* exhibited a similar upturn in cell size – also within the middle of the experimental range for N supply (Figure 5F). There was no strong evidence for any prior downwards trend with N stress (Figures 5F, S8P, S8Q, S12B and S12F). The upturn in cell size preceded TFA induction (N_i/L = 5.1 cf. 3.9) (Figures 5F cf. 5B) (Table 2).

In *N. oceanica* however, N stress associated with a prolonged trend of cell size reduction, well beyond the break point for TFA induction (N_i/L = 5.7) (Figure 5E cf. 5A) (Table 2). This downward trend coincided with increasing TFP, culminating in the highest oil productivity (TFP) condition (#31) which was also close to minimum cell size (Figure 5E). A single data point (#29) suggested an upturn might be occurring with extreme N stress (e.g. possible break point N_i/L = 1.4; near #31 in Figure 5E). A similar pattern was seen with the 3 independent measures of N stress: N_i (Figure S8N), DIN and PON (Figures S12A and S12E). The maximum N stress condition #29 (N_i/L = 0.04, input N/P ratio) gave very high TFA (80 %DW) but low TFP (17 $mgL^{-1}d^{-1}$) (Data S1).

With *C. vulgaris*, CH content correlated inversely with cell size (R^2 0.6), giving a threshold type response curve (Figure S11H), but there was no discernible relationship with TFA (Figure S11F). Conversely, in *N. oceanica*, there was a trend of decreasing cell size with increasing TFA content followed by an upturn (break point TFA 36% DW) leading to large cells with high oil (Figure S11E) but there was no clear trend for cell size with CH content (Figure S11G).

In summary, maximizing oil productivity was linked to small cell size and this could be due to improved light absorption. In *N. oceanica*, maintaining a small cell size was achieved by a low N/P input ratio. These were the same conditions that favored TFA accumulation over CH. It appeared that higher P status was required to prevent cell size increase, whereas low N was not linked strongly to cell size increases. In the case of *C.*

vulgaris, combined N and P stress led to high TFP where, to an extent, small cell size was maintained. However, CH was preferentially induced as an intermediate stress product, with TFA induction requiring higher stress levels. Therefore, TFP optimization was more constrained in this alga, with the approach taken here.

DISCUSSION

Large-scale culture of microalgae for oil might benefit from employing a semicontinuous culture system to boost productivity. Limited success so far has suggested that a better understanding of metabolic and physiological regulatory processes was needed. To search for a solution, we used PBR arrays to compare 2 high oil-producing marine strains from two distinct lineages under a matrix of variable growth conditions. This was complemented by extensive measurements of nutrient status to model and explain regulatory processes under pseudo steady-state conditions. The optimization process revealed that greater lipid productivity was achievable in *N. oceanica*, under semicontinuous culture, at 54 $mgL^{-1}d^{-1}$ (with >50% DW TFA) cf. *C. vulgaris* 40 $mgL^{-1}d^{-1}$ (with >40% DW TFA). The latter species was more predisposed to carbohydrate production, and it was harder to find conditions to diminish this competing storage product (max. levels 90 $mgL^{-1}d^{-1}$ at 45% DW cf. 22 $mgL^{-1}d^{-1}$ at 18% DW), despite both algae being high oil producers under batch cultivation (Slocombe et al., 2015). Our analysis of the underlying causes of these species-specific differences identified three key findings that have significant ramifications for boosting oil productivity generally in algae:

(i) Suppression of carbohydrate by high N/P ratio

We found that *N. oceanica* carbohydrate was primarily induced by P stress, whereas N stress was more effective for oil (in both algae). So, implementing a low N/P input ratio can suppress carbohydrate, maximizing oil. This strategy was less effective in *C. vulgaris* firstly, because both storage products showed a synergistic dependency on N stress and P stress and secondly, because carbohydrate was induced preferentially as an intermediate-stress product. This suggests that oil production is less readily optimized in continuous systems by manipulation of N/P ratio or by using graded nutrient stress for certain algal species. Our findings are consistent with oil being partly derived from a carbohydrate intermediate product in certain green algae (Li et al., 2015) and for direct synthesis of oil (TAG) in *N. oceanica* (Suen et al., 1987). Green algae accumulate starch, regulated variously by circadian rhythm as in higher plants or N depletion (Graf et al., 2010; Li et al., 2015; Ral et al., 2006), whereas heterokonts, such as *N. oceanica*, accumulate β-1,3-glucans (e.g. leucosin) instead (Li et al., 2014; Volkman et al., 1993).

(ii) Low stress thresholds for oil induction

Several independent measures of nutrient-depletion status revealed stress thresholds for oil to be 2–8 times less in *N. oceanica* compared with *C. vulgaris*. This favored high oil productivity under semicontinuous culture where high stresses that compromise growth must be avoided. In contrast, under batch culture, which is characterized by rapid increases in nutrient stress, *C. vulgaris* was equally effective in oil accumulation (Slocombe et al., 2015). In effect, N depletion from the medium was less in *N. oceanica* despite it producing more oil. We showed that oil induction was primarily due to the N supply restriction, however. Our threshold model suggested that *N. oceanica* prioritized oil over N assimilation and this was consistent with observations that a restriction on N assimilation rates can set high oil levels in this genus (Ajjawi et al., 2017). In comparison, P depletion from the medium was often near-complete in both species, despite growth being N- or light-limited under most conditions, suggesting luxury P storage (Chu et al., 2015; Singh et al., 2018). P supply appeared to be more influential for carbohydrate content or cell size in both species; the latter befitting the role of phosphate in cell cycle progression (Jiménez et al., 2015).

(iii) High stress thresholds for cell size increases

In *N. oceanica*, a high N-stress threshold for cell-size increase was evident. This led to a prolonged decrease in cell size with increasing N stress, combined with increasing oil accumulation. We suggest that the decrease in cell size is responsible for maximizing oil productivity, as follows. Firstly, there is an association of high oil productivity with small-celled algae gained from cross-species observations (Shurin et al., 2013; Slocombe et al., 2015), and we found here that semicontinuous growth conditions giving high oil productivity were linked to small cell size in both algae. Secondly, we noted that high growth conditions led to less chl per cell if the cells were smaller. Theoretical expectations are that the increased surface area to volume ratio would improve light interception (Marañón, 2015). Therefore, we inferred that reduction in cell size favored high oil productivity because the gain in light absorption permitted a reduced investment in photosynthetic capacity in favor of a proportionate increase in oil content, thus reducing the

impact on growth. Reduction in photosynthetic capacity under N limitation is associated with a diversion of C from photosynthetic PR into oil that is driven by low N availability (Ajjawi et al., 2017; Cazzaniga et al., 2014; Valenzuela et al., 2012; Vieler et al., 2012; Zienkiewicz et al., 2020). We noted a close inverse correlation between oil and chl in both species, in this regard.

The tendency of cell diameter in *N. oceanica* to downsize with N-stress leading to greater oil productivity was coupled with low N-depletion thresholds for oil induction. This would tend to mitigate N-limitation by reducing N assimilation and would push toward N supply and light colimitation, which was observed in *N. oceanica* under semicontinuous culture. With *C. vulgaris*, small cell size was more closely associated with high carbohydrate levels than it was with oil. Nevertheless, combined high oil content and oil productivity were still associated with small cell size in this species, and these could, to an extent, be elicited together by combined N and P stress (near-Redfield ratio, N/P = 19) for maximizing oil production.

Reports show P stress leading to larger cells and N stress to smaller cells in other microalgae which suggests that there are fundamental regulatory differences between the two nutrients (McKew et al., 2015; Olson et al., 1986; Peter and Sommer, 2013), and our findings indicate the process is complex. In most algae, the cell cycle is diurnal with reserves built up in the light, increasing cell volume, followed by division in the dark period (Zachleder et al., 2016). So, in theory, any stress that impedes growth will initially reduce the cell size attained prior to division. Eventually, further stress would trigger a delay in cell division which would lead to larger cells (McKew et al., 2015; Zachleder et al., 2016). We observed this pattern with increasing P stress in both species and likewise for N stress in *C. vulgaris*. In the case of *N. oceanica*, however, cell size reduction dominated in response to N stress and the switch to larger cells was delayed well beyond the stress levels needed to induce oil. Consequently, we found that low input N/P ratio acts in two ways to maximize oil productivity in this species by suppressing P-stress-mediated induction of both carbohydrate and large cell size, favoring N-stress-mediated oil induction along with cell size reduction.

The 3 key regulatory adaptations of *N. oceanica* that led toward high oil production under N stress probably related to its oceanic habitat which is characterized by stratified water columns. Here, N is colimiting with iron (Browning et al., 2017), and there is a need to prioritize oil as a buoyancy mechanism to counter sedimentation or for other survival/dispersal strategies (Sayanova et al., 2017). In this nutrient-poor habitat, small cell size poses a competitive advantage for nutrient uptake and further size reductions in response to N limitation would maximize surface area to volume ratio for nutrient absorption (Marañón, 2015; Marañón et al., 2013). Our data suggest that this adaptation leads to a similar advantage for light absorption under comparatively nutrient-rich conditions of algal culture, permitting oil accumulation and growth. In *C. vulgaris*, prioritizing oil production over N assimilation and photosynthetic capacity was less evident which, along with larger cell size, could account for the lesser light saturation and higher growth capacity that we observed compared with *N. oceanica* (Huete-Ortega et al., 2014; Marañón, 2015; Marañón et al., 2013). This, along with some benthic traits (we observed some surface adhesion) would be expected in nutrient-rich estuarine habitats (Underwood et al., 1998).

To achieve economic feasibility with low-value algal products such as oil for biofuel, feeds, and food, large-scale production must be geared toward continuous outputs. In a semicontinuous culture system, for instance, nutrient stresses, which are typically used to induce oil, must avoid productivity penalties. This requires algal species that prioritize oil production. In this study, we narrow down and delineate key morphological, phylogenetic, ecological, and regulatory traits in the search for optimal oil production in algae.

Limitations of the study

These studies were carried out using controlled conditions in the laboratory, whereas upscaling in open ponds introduces additional seasonal, meteorological, diurnal, and biotic factors. Therefore, our optimizing conditions must be tested in this context to take full advantage of our findings. Although productivity levels were strong with the *N. oceanica* strain for instance, its presumed adaptation to impoverished environments (stratified waters) might lead to issues with upscaling in the outdoor environment with high nutrients. Small cell size can also lead to increased susceptibility to fast-growing predators (Hansson et al., 1998).

STAR★METHODS

Detailed methods are provided in the online version of this paper and include the following:

- KEY RESOURCES TABLE

SUPPLEMENTAL INFORMATION

Supplemental information can be found online at https://doi.org/10.1016/j.isci.2021.102743.

A video abstract is available at https://doi.org/10.1016/j.isci.2021.102743#mmc4.

A video abstract is available at https://doi.org/10.1016/j.isci.2021.102743#mmc5.

ACKNOWLEDGMENTS

We are very grateful to Debra Brennan and Elaine Mitchell for technical assistance at SAMS. All other members of the project consortium, who did not directly participate in this study, are gratefully acknowledged for their indirect contributions. This work is a result of the UKRI BBSRC-DBT funded UK-India SuBB project (BB/K020633/1). S.V. also acknowledges financial support from UKRI EPSRC (EP/E036252/1) to Sheffield.

AUTHOR CONTRIBUTIONS

S.V., M.H.-O., S.P.S., J.G.D., and M.S.S conceived and planned the project. S.V., M.S.S., and J.G.D. (along with other members of the consortium) were responsible for funding acquisition. Experimental work was undertaken by S.P.S, M.H.-O., R.V.K., K.O., and A.M. Data analysis was carried out by S.P.S, R.V.K., M.H.-O., and S.V. The manuscript was written by S.P.S., M.H.-O., S.V., and R.V.K.

DECLARATION OF INTERESTS

The authors declare no competing interests.

Received: January 12, 2021
Revised: May 7, 2021
Accepted: June 14, 2021
Published: July 23, 2021

REFERENCES

Ajjawi, I., Verruto, J., Aqui, M., Soriaga, L.B., Coppersmith, J., Kwok, K., Peach, L., Orchard, E., Kalb, R., Xu, W., et al. (2017). Lipid production in *Nannochloropsis gaditana* is doubled by decreasing expression of a single transcriptional regulator. Nat. Biotechnol. *35*, 647–652. https://doi.org/10.1038/nbt.3865.

Benemann, J. (2013). Microalgae for biofuels and animal feeds. Energies *6*, 5869–5886. https://doi.org/10.3390/en6115869.

Benvenuti, G., Bosma, R., Ji, F., Lamers, P., Barbosa, M.J., and Wijffels, R.H. (2016). Batch and semi-continuous microalgal TAG production in lab-scale and outdoor photobioreactors. J. Appl. Phycol. *28*, 3167–3177. https://doi.org/10.1007/s10811-016-0897-1.

Bi, R., Arndt, C., and Sommer, U. (2014). Linking elements to biochemicals: effects of nutrient supply ratios and growth rates on fatty acid composition of phytoplankton species. J. Phycol. *50*, 117–130. https://doi.org/10.1111/jpy.12140.

Borowitzka, M.A., and Vonshak, A. (2017). Scaling up microalgal cultures to commercial scale. Eur. J. Phycol. https://doi.org/10.1080/09670262.2017.1365177.

Brito, V.L.G., Weynans, K., Sazima, M., and Lunau, K. (2015). Trees as huge flowers and flowers as oversized floral guides: the role of floral color

change and retention of old flowers in *Tibouchina pulchra*. Front. Plant Sci. *6*, 362. https://doi.org/10.3389/fpls.2015.00362.

Browning, T.J., Achterberg, E.P., Rapp, I., Engel, A., Bertrand, E.M., Tagliabue, A., and Moore, C.M. (2017). Nutrient co-limitation at the boundary of an oceanic gyre. Nature *551*, 242. https://doi.org/10.1038/nature24063.

Bull, A.T. (2010). The renaissance of continuous culture in the post-genomics age. J. Ind. Microbiol. Biotechnol. *37*, 993–1021. https://doi.org/10.1007/s10295-010-0816-4.

Butler, T.O., Acurio, K., Mukherjee, J., Dangasuk, M.M., Corona, O., and Vaidyanathan, S. (2021). The transition away from chemical flocculants: Commercially viable harvesting of *Phaeodactylum tricornutum*. Sep. Purif. Technol. *255*, 117733. https://doi.org/10.1016/j.seppur.2020.117733.

Campos, H., Boeing, W.J., Dungan, B.N., and Schaub, T. (2014). Cultivating the marine microalga *Nannochloropsis salina* under various nitrogen sources: effect on biovolume yields, lipid content and composition, and invasive organisms. Biomass Bioenergy *66*, 301–307. https://doi.org/10.1016/j.biombioe.2014.04.005.

Cazzaniga, S., Dall'Osto, L., Szaub, J., Scibilia, L., Ballottari, M., Purton, S., and Bassi, R. (2014). Domestication of the green alga *Chlorella sorokiniana*: reduction of antenna size improves light-use efficiency in a photobioreactor. Biotechnol. Biofuels *7*, 157. https://doi.org/10.1186/s13068-014-0157-z.

Chen, Y., and Vaidyanathan, S. (2012). A simple, reproducible and sensitive spectrophotometric method to estimate microalgal lipids. Anal. Chim. Acta *724*, 67–72. https://doi.org/10.1016/j.aca.2012.02.049.

Chen, Y., and Vaidyanathan, S. (2013). Simultaneous assay of pigments, carbohydrates, proteins and lipids in microalgae. Anal. Chim. Acta *776*, 31–40. https://doi.org/10.1016/j.aca.2013.03.005.

Chu, F.-F., Shen, X.-F., Lam, P.K.S., and Zeng, R.J. (2015). Polyphosphate during the Regreening of *Chlorella vulgaris* under nitrogen deficiency. Int. J. Mol. Sci. *16*, 23355–23368. https://doi.org/10.3390/ijms161023355.

Collos, Y., Mornet, F., Sciandra, A., Waser, N., Larson, A., and Harrison, P.J. (1999). An optical method for the rapid measurement of micromolar concentrations of nitrate in marine phytoplankton cultures. J. Appl. Phycol. *11*, 179–184. https://doi.org/10.1023/A:1008046023487.

Danquah, M., Ang, L., Uduman, N., Moheimani, N., and Forde, G. (2009). Dewatering of microalgal culture for biodiesel production: Exploring polymer flocculation and tangential flow filtration. J. Chem. Technol. Biotechnol. *84*, 1078–1083. https://doi.org/10.1002/jctb.2137.

Day, J.G., Slocombe, S.P., and Stanley, M.S. (2012). Overcoming biological constraints to enable the exploitation of microalgae for biofuels. Bioresour. Technol. *109*, 245–251. https://doi.org/10.1016/j.biortech.2011.05.033.

Dyble, M., Narendran, N., Bierman, A., and Klein, T. (2005). Impact of dimming white LEDs: chromaticity shifts due to different dimming methods. Proc. SPIE, 5941. https://doi.org/10.1117/12.625924.

Fukuda, S., Hirasawa, E., Takemura, T., Takahashi, S., Chokshi, K., Pancha, I., Tanaka, K., and Imamura, S. (2018). Accelerated triacylglycerol production without growth inhibition by overexpression of a glycerol-3-phosphate acyltransferase in the unicellular red alga *Cyanidioschyzon merolae*. Sci. Rep. *8*, 12410. https://doi.org/10.1038/s41598-018-30809-8.

Georgianna, D.R., and Mayfield, S.P. (2012). Exploiting diversity and synthetic biology for the production of algal biofuels. Nature *488*, 329–335. https://doi.org/10.1038/nature11479.

Goswami, G., Kumar, R., Sinha, A., Maiti, S.K., Dutta, B.C., Singh, H., and Das, D. (2019). A low-cost and scalable process for harvesting microalgae using commercial-grade flocculant. RSC Adv. *9*, 39011–39024. https://doi.org/10.1039/c9ra08072d.

Graf, A., Schlereth, A., Stitt, M., and Smith, A.M. (2010). Circadian control of carbohydrate availability for growth in Arabidopsis plants at night. Proc. Natl. Acad. Sci. U S A *107*, 9458–9463. https://doi.org/10.1073/pnas.0914299107.

Greenwell, H.C., Laurens, L.M.L., Shields, R.J., Lovitt, R.W., and Flynn, K.J. (2010). Placing microalgae on the biofuels priority list: a review of the technological challenges. J. R. Soc. Interfaces *7*, 703–726. https://doi.org/10.1098/rsif.2009.0322.

Hammer, Ø., Harper, D.A.T., and Ryan, P.D. (2001). PAST: Paleontological Statistics software packages for education and data analysis. Palaeontol. Electron. *4*, 1–9.

Hansson, L.-A., Bergman, E., and Cronberg, G. (1998). Size structure and succession in phytoplankton communities: the impact of interactions between herbivory and predation. Oikos *81*, 337–345. https://doi.org/10.2307/3547054.

Huang, X., Huang, Z., Wen, W., and Yan, J. (2013). Effects of nitrogen supplementation of the culture medium on the growth, total lipid content and fatty acid profiles of three microalgae (*Tetraselmis subcordiformis, Nannochloropsis oculata* and *Pavlova viridis*). J. Appl. Phycol. *25*, 129–137. https://doi.org/10.1007/s10811-012-9846-9.

Huete-Ortega, M., Rodríguez-Ramos, T., DC, L.-S., Cermeño, P., JM, B., RL, P., Rodríguez, J., and Marañón, E. (2014). Distinct patterns in the size-scaling of abundance and metabolism in coastal and open-ocean phytoplankton communities. *Mar.* Ecol. Prog. Ser. *515*, 61–71. https://www.int-res.com/abstracts/meps/v515/p61-71/.

Jiménez, J., Bru, S., Ribeiro, M., and Clotet, J. (2015). Live fast, die soon: cell cycle progression and lifespan in yeast cells. Microb. Cell *2*, 62–67. https://doi.org/10.15698/mic2015.03.191.

Kapoore, R.V., Huete-Ortega, M., Day, J.G., Okurowska, K., Slocombe, S.P., Stanley, M.S., and Vaidyanathan, S. (2019). Effects of cryopreservation on viability and functional stability of an industrially relevant alga. Sci. Rep. *9*, 1–12. https://doi.org/10.1038/s41598-019-38588-6.

Klok, A.J., Lamers, P.P., Martens, D.E., Draaisma, R.B., and Wijffels, R.H. (2014). Edible oils from microalgae: insights in TAG accumulation. Trends Biotechnol. *32*, 521–528. https://doi.org/10.1016/j.tibtech.2014.07.004.

Li, J., Han, D., Wang, D., Ning, K., Jia, J., Wei, L., Jing, X., Huang, S., Chen, J., Li, Y., et al. (2014). Choreography of transcriptomes and lipidomes of *Nannochloropsis* reveals the mechanisms of oil synthesis in microalgae. Plant Cell *26*, 1645–1665. https://doi.org/10.1105/tpc.113.121418.

Li, T., Gargouri, M., Feng, J., Park, J.-J., Gao, D., Miao, C., Dong, T., Gang, D.R., and Chen, S. (2015). Regulation of starch and lipid accumulation in a microalga *Chlorella sorokiniana*. Bioresour. Technol. *180*, 250–257. https://doi.org/10.1016/j.biortech.2015.01.005.

Marañón, E. (2015). Cell size as a key determinant of phytoplankton metabolism and community structure. Ann. Rev. Mar. Sci. *7*, 241–264. https://doi.org/10.1146/annurev-marine-010814-015955.

Marañón, E., Cermeño, P., López-Sandoval, D.C., Rodríguez-Ramos, T., Sobrino, C., Huete-Ortega, M., Blanco, J.M., and Rodríguez, J. (2013). Unimodal size scaling of phytoplankton growth and the size dependence of nutrient uptake and use. Ecol. Lett. *16*, 371–379. https://doi.org/10.1111/ele.12052.

Mata, T.M., Martins, A.A., and Caetano, N.S. (2010). Microalgae for biodiesel production and other applications: a review. Renew. Sustain. Energy Rev. *14*, 217–232. https://doi.org/10.1016/j.rser.2009.07.020.

Mathimani, T., Baldinelli, A., Rajendran, K., Prabakar, D., Manickam, M., van Leeuwen, R., and Pugazhendhi, A. (2018). Review on cultivation and thermochemical conversion of microalgae to fuels and chemicals: process evaluation and knowledge gaps. J. Clean. Prod. *208*, 1053–1064. https://doi.org/10.1016/j.jclepro.2018.10.096.

McKew, B.A., Metodieva, G., Raines, C.A., Metodiev, M.V., and Geider, R.J. (2015). Acclimation of *Emiliania huxleyi* (1516) to nutrient limitation involves precise modification of the proteome to scavenge alternative sources of N and P. Environ. Microbiol. *17*, 4050–4062. https://doi.org/10.1111/1462-2920.12957.

Negi, S., Perrine, Z., Friedland, N., Kumar, A., Tokutsu, R., Minagawa, J., Berg, H., Barry, A.N., Govindjee, G., and Sayre, R. (2020). Light regulation of light-harvesting antenna size substantially enhances photosynthetic efficiency and biomass yield in green algae. Plant J. *103*, 584–603. https://doi.org/10.1111/tpj.14751.

Ngan, C.Y., Wong, C.H., Choi, C., Yoshinaga, Y., Louie, K., Jia, J., Chen, C., Bowen, B., Cheng, H., Leonelli, L., et al. (2015). Lineage-specific chromatin signatures reveal a regulator of lipid metabolism in microalgae. Nat. Plants *1*, 1–25. https://doi.org/10.1038/nplants.2015.107.

Olson, R.J., Vaulot, D., and Chisholm, S.W. (1986). Effects of environmental stresses on the cell cycle of two marine phytoplankton species. Plant Physiol. *80*, 918–925. https://doi.org/10.1104/pp.80.4.918.

Park, J.B.K., Craggs, R.J., and Shilton, A.N. (2011). Wastewater treatment high rate algal ponds for biofuel production. Bioresour. Technol. *102*, 35–42. https://doi.org/10.1016/j.biortech.2010.06.158.

Park, S., Steen, C.J., Lyska, D., Fischer, A.L., Endelman, B., Iwai, M., Niyogi, K.K., and Fleming, G.R. (2019). Chlorophyll-carotenoid excitation energy transfer and charge transfer in *Nannochloropsis oceanica* for the regulation of photosynthesis. Proc. Natl. Acad. Sci. U S A *116*, 3385–3390. https://doi.org/10.1073/pnas.1819011116.

Peter, K.H., and Sommer, U. (2013). Phytoplankton cell size reduction in response to warming mediated by nutrient limitation. PLoS One *8*, 1–6. https://doi.org/10.1371/journal.pone.0071528.

Piepho, M., Arts, M.T., and Wacker, A. (2012). Species-specific variation in fatty acid concentrations of four phytoplankton species: does phosphorus supply influence the effect of light intensity or temperature? J. Phycol. *48*, 64–73. https://doi.org/10.1111/j.1529-8817.2011.01103.x.

Přibyl, P., Cepák, V., and Zachleder, V. (2012). Production of lipids in 10 strains of *Chlorella* and *Parachlorella*, and enhanced lipid productivity in *Chlorella vulgaris*. Appl. Microbiol. Biotechnol. *94*, 549–561. https://doi.org/10.1007/s00253-012-3915-5.

Prioretti, L., Carriere, F., Field, B., Avilan, L., Montané, M.H., Menand, B., and Gontero, B. (2020). Targeting TOR signaling for enhanced lipid productivity in algae. Biochimie *169*, 12–17. https://doi.org/10.1016/j.biochi.2019.06.016.

Ral, J.-P., Colleoni, C., Wattebled, F., Dauvillée, D., Nempont, C., Deschamps, P., Li, Z., Morell, M., Chibbar, R., Purton, S., et al. (2006). Circadian clock regulation of starch metabolism establishes GBSSI as a major contributor to amylopectin synthesis in *Chlamydomonas reinhardtii*. Plant Physiol. *142*, 305–317. https://doi.org/10.1104/pp.106.081885.

Sayanova, O., Mimouni, V., Ulmann, L., Morant-Manceau, A., Pasquet, V., Schoefs, B., and Napier, J.A. (2017). Modulation of lipid biosynthesis by stress in diatoms. Phil. Trans. R. Soc. B *372*, 20160407. https://doi.org/10.1098/rstb.2016.0407.

Shurin, J.B., Abbott, R.L., Deal, M.S., Kwan, G.T., Litchman, E., McBride, R.C., Mandal, S., and Smith, V.H. (2013). Industrial-strength ecology: trade-offs and opportunities in algal biofuel production. Ecol. Lett. *16*, 1393–1404. https://doi.org/10.1111/ele.12176.

Singh, D., Nedbal, L., and Ebenhöh, O. (2018). Modelling phosphorus uptake in microalgae. Biochem. Soc. Trans. *46*, 483–490. https://doi.org/10.1042/BST20170262.

Slocombe, S.P., Ross, M., Thomas, N., McNeill, S., and Stanley, M.S. (2013a). A rapid and general method for measurement of protein in micro-algal biomass. Bioresour. Technol. *129*, 51–57. https://doi.org/10.1016/j.biortech.2012.10.163.

Slocombe, S.P., Zhang, Q., Black, K.D., Day, J.G., and Stanley, M.S. (2013b). Comparison of screening methods for high-throughput determination of oil yields in micro-algal biofuel strains. J. Appl. Phycol. *25*, 961–972. https://doi.org/10.1007/s10811-012-9947-5.

Slocombe, S.P., Zhang, Q., Ross, M., Stanley, M.S., and Day, J.G. (2016). Screening and improvement of marine microalgae for oil production. In Microalgal Production for Biomass and High-Value Products, S.P. Slocombe and J.R. Benemann, eds. (CRC Press), pp. 91–112. http://www.crcnetbase.com/isbn/978-1-4822-1970-8.

Slocombe, S.P., Zhang, Q., Ross, M., Anderson, A., Thomas, N.J., Lapresa, Á., Rad-Menéndez, C., Campbell, C.N., Black, K.D., Stanley, M.S., and Day, J.G. (2015). Unlocking nature's treasure-chest: screening for oleaginous algae. Sci. Rep. *5*, 1–17. https://doi.org/10.1038/srep09844.

Solorzano, L., and Sharp, J.H. (1980). Determination of total dissolved phosphorus particulate phosphorus in natural water. Limnol. Oceanogr. *25*, 754–758. https://doi.org/10.4319/lo.1980.25.4.0754.

Stephens, E., Ross, I.L., Mussgnug, J.H., Wagner, L.D., Borowitzka, M.a., Posten, C., Kruse, O., and Hankamer, B. (2010). Future prospects of microalgal biofuel production systems. Trends Plant Sci. *15*, 554–564. https://doi.org/10.1016/j.tplants.2010.06.003.

Strickland, J.D.H., and Parsons, T.R. (1968). A manual for sea water analysis. Bull. Fish. Res. Bd. Can. *167*, 49–64.

Suen, Y., Hubbard, J.S., Holzer, G., and Tornabene, T.G. (1987). Total lipid production of the green alga *Nannochloropsis* sp. QII under different nitrogen regimes. J. Phycol. *296*, 289–296. https://doi.org/10.1111/j.1529-8817.1987.tb04137.x.

Takagi, M., Karseno, and Yoshida, T. (2006). Effect of salt concentration on intracellular accumulation of lipids and triacylglyceride in marine microalgae *Dunaliella* cells. J. Biosci. Bioeng. *101*, 223–226. https://doi.org/10.1263/jbb.101.223.

Tseng, Y.H., Mohanty, S.K., McLennan, J.D., and Pease, L.F. (2019). Algal lipid extraction using confined impinging jet mixers. Chem. Eng. Sci. X *1*, 100002. https://doi.org/10.1016/j.cesx.2018.100002.

Underwood, G.J.C., Phillips, J., and Saunders, K. (1998). Distribution of estuarine benthic diatom species along salinity and nutrient gradients. Eur. J. Phycol. *33*, 173–183.

Valenzuela, J., Mazurie, A., Carlson, R.P., Gerlach, R., Cooksey, K.E., Peyton, B.M., and Fields, M.W. (2012). Potential role of multiple carbon fixation pathways during lipid accumulation in *Phaeodactylum tricornutum*. Biotechnol. Biofuels *5*, 40. https://doi.org/10.1186/1754-6834-5-40.

Vieler, A., Wu, G., Tsai, C.-H., Bullard, B., Cornish, A.J., Harvey, C., Reca, I.-B., Thornburg, C., Achawanantakun, R., Buehl, C.J., et al. (2012). Genome, functional gene annotation, and nuclear transformation of the heterokont oleaginous alga *Nannochloropsis oceanica* CCMP1779. PLoS Genet. *8*, e1003064. https://doi.org/10.1371/journal.pgen.1003064.

Volkman, J.K., Brown, M.R., Dunstan, G.A., and Jeffrey, S.W. (1993). The biochemical composition of marine microalgae from the class Eustigmatophyceae. J. Phycol. *29*, 69–78. https://doi.org/10.1111/j.1529-8817.1993.tb00281.x.

Wetherwax, P.B. (1986). Why do honeybees reject certain flowers? Oecologia *69*, 567–570. http://www.jstor.org/stable/4217986.

Wijffels, R.H., and Barbosa, M.J. (2010). An outlook on microalgal biofuels. Science *329*, 796–799. https://doi.org/10.1126/science.1189003.

Williams, P.J., le, B., and Laurens, L.M.L. (2010). Microalgae as biodiesel & biomass feedstocks: review & analysis of the biochemistry, energetics & economics. Energy Environ. Sci. *3*, 554–590. https://doi.org/10.1039/b924978h.

Zachleder, V., Bisova, K., and Vitova, M. (2016). The cell cycle of microalgae. In The Physiology of Microalgae, M.A. Borowitzka, J. Beardall, and J.A. Raven, eds. (Springer), pp. 3–46. https://doi.org/10.1007/978-3-319-24945-2.

Zienkiewicz, A., Zienkiewicz, K., Poliner, E., Pulman, J.A., Du, Z.-Y., Stefano, G., Tsai, C.-H., Horn, P., Feussner, I., Farre, E.M., et al. (2020). The microalga *Nannochloropsis* during transition from quiescence to autotrophy in response to nitrogen availability. Plant Physiol. *182*, 819–839. https://doi.org/10.1104/pp.19.00854.

STAR★METHODS

KEY RESOURCES TABLE

REAGENT or RESOURCE	SOURCE	IDENTIFIER
Chemicals, peptides, and recombinant proteins		
Glass beads, acid-washed 425-600 μm (30-40 U.S. sieve)	Sigma	Cat#G8772
Critical commercial assays		
Pierce™ BCA Protein Assay Kit	ThermoFisher Scientific	Cat# 23225
Experimental models: Organisms/strains		
Nannochloropsis oceanica CCAP 849/10	https://www.ccap.ac.uk/catalogue/strain-849-10?search=CCAP%20849%2F10	CCAP 849/10
Chorella vulgaris CCAP 221/21A	https://www.ccap.ac.uk/catalogue/strain-211-21A?search=211%2F21A	CCAP 211/21A
Software and algorithms		
Image J	National Institutes of Health (NIH)	https://imagej.nih.gov/ij/
Design Expert 10	StatEase	https://www.statease.com/software/design-expert/
PAST: PALEONTOLOGICAL STATISTICS SOFTWARE PACKAGE FOR EDUCATION AND DATA ANALYSIS	Hammer et al., 2001	https://palaeo-electronica.org/2001_1/past/issue1_01.htm
NCSS12 Data Analysis & Graphics	NCSS Statistical Softare	https://www.ncss.com/download/ncss/updates/ncss-12/
MATLAB	MathWorks	https://uk.mathworks.com/products/matlab.html
Wolfram Alpha Widgets: cubic equation solver	Wolfram Alpha	https://www.wolframalpha.com/widgets/view.jsp?id=3f4366aeb9c157cf9a30c90693eafc55
Other		
Quantum scalar irradiance light meter	Biospherical Instruments Inc., San Diego, CF	http://www.biospherical.com/index.php?option=com_content&view=article&id=50&Itemid=88
Direct Variable Area Flow Meter (0.04 L/min → 0.5 L/min, RS)	RS	Cat# 198-2975
Qiagen Tissue Lyser	Qiagen	https://www.qiagen.com/us/products/human-id-and-forensics/automation/tissuelyser-ii/
Coulter Counter	BeckmanCoulter	https://www.beckman.com/cell-counters-and-analyzers/multisizer-3

RESOURCE AVAILABILITY

Lead contact

Further information and requests for resources should be directed to and will be fulfilled by the Lead Contact, Seetharaman Vaidyanathan (s.vaidyanathan@sheffield.ac.uk).

Materials availability

This study did not generate new unique reagents.

Data and code availability

The data generated during this study are available as supplementary information.

EXPERIMENTAL MODEL AND SUBJECT DETAILS

Nannochloropsis oceanica (CCAP 849/10) and the "marine" *Chlorella vulgaris* strain (CCAP 211/21A) were from CCAP, UK www.ccap.ac.uk and were grown in an artificial seawater-based f/2 medium as described

(Slocombe et al., 2015) and shown here: 33.5 g/L Instant Ocean (Aquarium Systems, France) pH adjusted to 6.9-7.0; the following added to final conc. 75mg/L $NaNO_3$, 5.65mg/L $NaH_2PO_4.2H_2O$, trace metals (final conc. Na_2EDTA 4.16mg/L, $FeCl_3.6H_2O$ 3.15mg/L, $CuSO_4.5H_2O$ 0.01mg/L, $ZnSO_4.7H_2O$ 0.022mg/L, $CoCl_2.7H_2O$ 0.01mg/L, $MnCl_2.4H_2O$ 0.18mg/L, Na_2MoO_4 $.2H_2O$ 0.006mg/L) Tris-base to 1mM, pH adjusted to 6.8-7.0; vitamins (final conc. Cyanocobalamin 0.5µg/L, Biotin 0.5µg/L; Thiamine-HCl 0.1mg/L) were added after autoclaving. For salinity tolerance testing, algae were grown in 24-well tissue-culture plates as 2 mL cultures under a 16 h:8 h light/dark regime at 50-80 $\mu Em^{-2}\ s^{-1}$ at 20°C for 7 d (Innova 44, New Brunswick Scientific, Edison, NJ). The salinity of the f/2 medium was taken as 0.3M and adjusted upwards by the addition of 5M NaCl stock.

All further algal culture experiments were carried out in multi-PBR arrays where some of the f/2 medium trace metal and vitamin final concentrations were set higher to avoid growth limitation: Cyanocobalamin 5µg/L; $CuSO_4.5H_2O$ 0.08 mg/L, $ZnSO_4.7H_2O$ 0.22 mg/L, $CoCl_2.6H_2O$ 0.08 mg/L, 1.81 mg/L $MnCl_2.4H_2O$ 1.81 mg/L, $Na_2MoO_4.2H_2O$ 0.39 mg/L. Buffering with 30 mM HEPES (pH 7.2) was used to prevent washout under semi-continuous culture due to lowering of pH with CO_2, which was observed to happen under certain conditions with *N. oceanica*. Nitrate and phosphate levels were adjusted according to the treatments (Table S1, S2).

METHOD DETAILS

PBR multi-arrays

These consisted of multiple custom-made units of 10 x 0.5L PBRs placed in dark controlled temperature environments at 25°C (Figures S1D and S1E). The light was provided by vertical panel housing cool white LEDs strips dimmed to achieve each experimental irradiance. Spectral shifts due to electrical dimming were not considered but these have been found to be minimal with white LEDs compared with RGB systems (Dyble et al., 2005). Different CO_2 levels were supplied by mixing compressed air and CO_2 (1–-100%, BOC). Aeration was achieved with pore size 3 spargers (Duran) with prior filtration (0.22 µm, Millipore) and delivered at 100 cc per min (0.2 vvm) with a Direct Variable Area Flow Meter (0.04 L/min → 0.5 L/min, RS) at each PBR. Light levels were measured inside the center of the culture tube in medium using a quantum scalar irradiance light meter (Biospherical Instruments Inc., San Diego, CF).

Experimental design

In order to optimize parameters for oil production using surface-response methodology, PBR multi-arrays were run with input variables of light, CO_2, nitrate and phosphate according to a matrix of 30 core conditions generated using Central Composite Design (Design Expert 7, Stat-Ease) (Table S1). Additional combinations (#31-33) were added manually. Input variables were light (40-300 $\mu mol\ m^{-2}s^{-1}$), CO_2 (0.04-4% vol.), stock nitrate (N_s) (50-5000 µM) and phosphate (P_s) concentration (4-264 µM) (Table S2). Values were selected after a literature survey to range from limiting conditions to super-saturating (Table S2) (Bi et al., 2014; McKew et al., 2015). Included in the core matrix were 6 centre point controls (#2,3,5,6,13,26) where the 4 input variables were set to median values. A further dilution factor ($\%\mu_{MAX}$) was assigned for semi-continuous culture based on growth factor-limitation (Table S1) where $\%\mu_{MAX}$ and the 4 input variables were independent (Table S4). The matrix resulted in 6 different off-Redfield input N/P ratios along with the near-Redfield ratio (=19). Approximately half of the conditions gave a near-Redfield molar N/P input ratio and were judged to be sufficient/saturating and the remainder were judged limiting (Table S1). Nutrient supply rates (N_i and P_i) were the product of N_s (or P_s) and replacement volume (RV) where N_i and P_i co-correlated (r_s >0.7; p<0.001), being dependent on operational rate (OR) (r_s >0.8; p<0.001) (Table S4). RV and OR both derived from μ_{MAX} and $\%\mu_{MAX}$ (see below), where μ_{MAX} was light-dependent in both species (r_s >0.6, p<0.001) (Table S4).

Semi-continuous culture

Maximum growth rates (μ_{MAX}) were determined for conditions #1-31 in batch mode to set OR under semi-continuous culture. μ_{MAX} was obtained from a plot of $Log_e\ A_{595}$ v. time, with the inoculum diluted to 0.15 A_{595}. Cultures were grown in semi-continuous chemostat mode after growth to late-log phase, with a daily fixed replacement volume (RV). This was undertaken 4 h into the light period (defined as the "endpoint") of a 16 h: 8 h light/dark diurnal cycle and was calculated as follows:

$$RV = \text{Culture vol} \cdot (1\text{-}1/e^{(OR)}) \text{ where } OR = \mu_{MAX} \cdot \%\mu_{MAX}$$

Under replete/sub-saturating conditions $\%\mu_{MAX} \leq 80\%$ and for limiting conditions $\%\mu_{MAX} \leq 20\%$, based on the literature (Bi et al., 2014; McKew et al., 2015) (Table S1); where lower $\%\mu_{MAX}$ values were used to avoid washout. Once steady state was achieved, cultures were grown for ≥ 5 generations to ensure acclimation before sampling at the endpoint for ≥ 3 consecutive days.

Harvesting samples

The algal culture was harvested by retaining ≤ 50 mL aliquots during endpoint medium replacement, recording the volumes. Biomass was recovered by centrifugation (4000g 15 min) in 50 mL tubes after cooling. Supernatant from one aliquot was retained (≤ 5 mL) and passed through a filter (0.22 μm, Millipore) and stored (-20°C). Pellets were rinsed to remove medium and re-spun in 1.5 mL screw-capped Eppendorf tubes prior to flash-freezing in liquid N_2 and freeze-drying followed by storage (-80°C). DW was recorded allowing BMP to be calculated (g DW L^{-1} d^{-1}).

Elemental analysis measurements

From the freeze-dried biomass samples, total C and N levels (termed Particulate Organic Carbon, POC and Particulate Organic Nitrogen, PON) were measured using an ANCA-GSL 20-20 stable isotope analyzer (PDZ Europa, Sercon Ltd., Crewe, UK). Freeze-dried samples at 1–2 mg micro-algal DW biomass were combusted in pre-weighed aluminum capsules with helium as a carrier gas. The instrument was calibrated using l-isoleucine standards (Sigma) over the range 5–200 μg N and 33–1320 μg C, delta calibrated N-7.89, C-12.18 (Slocombe et al., 2013a, 2013b).

Oil content measurements

Oil content was assessed by measuring Total Fatty Acids (TFA) by GC-FID with direct-derivatization (Kapoore et al., 2019; Slocombe et al., 2013a, 2013b) and comparing with C/N ratio and FA unsaturation/saturation ratio. A composite oil proxy (TFA_{CR}) was generated from the above 3 oil proxies and utilized for data analysis of oil content in place of TFA where necessary (see Figure S13).

Multi-assay procedure

A multi-assay procedure (Chen and Vaidyanathan, 2012, 2013) was modified for large scale operation, for total protein, carbohydrate, chlorophyll and carotenoids as follows. Dry pellets (1-1.5 mg) were resuspended in 24 μL of the phosphate buffer (0.05 M Potassium di-hydrogen phosphate to pH to 7.4 with KOH) and 1.8 mL of 25% (v/v) methanol in 1N of NaOH in 2.0 mL screw-capped Eppendorf tubes. After the addition of 0.1-0.2 mL of acid-washed 425-600μm glass beads (Sigma), resuspended pellets were homogenized in a bead-beater (30 min.) (Qiagen Lyser, Qiagen).

For carbohydrate, 2 aliquots of 0.2 mL extract were transferred to glass vials after vortexing: for the control with addition of 1.2 mL 75% H_2SO_4; for the experimental sample with 0.4 mL 75% H_2SO_4 and 0.8 mL anthrone reagent (freshly prepared: 50 mg anthrone (Sigma) plus 1 mL EtOH plus 25 mL 75% Sulfuric Acid). After incubation at 100°C 15 min, and cooled to RT the absorbance was measured in polystyrene cuvettes (ΔA_{630}). Glucose standards were used at 0.01-1 mg/mL.

The remainder of the extract was stored at -80°C and later saponified (30 min 100°C) for all further assays. For the protein assay, saponified extracts of 10 μL (avoided floating material) were first placed directly into 96-well assay plates with the following additions: controls, 0.2 mL BCA reagent alone (Thermo Scientific); experimental, 0.2 mL BCA/Cu mix (Thermo Scientific) and incubated at 37°C for 1 h, measuring ΔA_{560}. A BSA standard (200 mg/mL stock, Sigma) was used at 0.01-3 mg/mL.

The remainder of the saponified extract was stored at -80°C for subsequent pigment assay where after vortexing, 0.7 mL was removed into 2 mL screw-cap Eppendorf tubes, adding 1.05 mL buffer R2 (chloroform: methanol 2:1, v/v) for phase separation (vortex, centrifuge 10 min.). The top phase (chlorophyll) was removed into a screw-cap Eppendorf and the lower phase (carotenoids) transferred into a separate tube. For chlorophyll, 0.6 mL was placed in 1 mL (2 mm) quartz cuvette for OD readings at 416, 453 and 750 nm or 0.2 mL in a 96-well UV plate (Fisher) (Chen & Vaidyanathan, 2012, 2013). The cuvette was cleaned with methanol for the next chlorophyll sample. For carotenoids, 0.6 mL was transferred to 1 mL (2 mm) quartz cuvette for OD 450 and 750 nm, cleaning the cuvette in R2 buffer between samples. Pigment concentrations were calculated according to the following formulas (Chen and Vaidyanathan, 2013):

$$C_a = 6.40 \cdot (A_{416} - A_{750}) - 0.79 \cdot (A_{453} - A_{750})$$

$$C_b = 5.87 \cdot (A_{453} - A_{750}) - 0.24 \cdot (A_{416} - A_{750})$$

$$C_{car} = 7.33 \cdot (A_{450} - A_{750})$$

Where C_a, C_b and C_{car} represent concentrations of Chla, Chlb and total carotenoids in μg/mL with 1 cm pathlength used.

Inorganic anion measurements

High-throughput assays for phosphate measurements were carried out using methods based on Strickland and Parsons (described below for 96-well assay plates) (Strickland and Parsons, 1968), where biomass levels were referred to as Particulate Organic Phosphorus (POP, %DW) and medium levels were referred to as Dissolved Inorganic Phosphate (DIP, μM).

Hence POP was determined on 1 mg of dried biomass as described (Solorzano and Sharp, 1980) with modifications, as follows. Pellets were twice resuspended in 1 mL Na_2SO_4 (0.17M) and centrifuged at 4000g for 5-10 min followed by resuspension in 2 mL $MgSO_4$ (0.017M). After transfer to a 10-15 mL glass vial, samples were dried at 60°C O/N and heated in a muffle furnace for 2 h, 475°C. After cooling, 5 ml HCL (0.2M) was added with incubation for 30 min at 80°C. From undisturbed samples, 100 μL was added into 100 μL water, pre-pipetted into 96-well assay plates.

In the case of the DIP measurements, 0.2 mL filtered endpoint medium (prepared as above) was added directly to the plates. Standards were prepared by serial dilutions of 16 mM NaH_2PO_4 and, in the case of POP only, a final conc. of 0.1M HCl was included.

For both POP and DIP samples, the assay was initiated by adding 20 μL of fresh reagent mix, prepared as follows (Strickland and Parsons, 1968). Fresh reagent mix was prepared in volumetric ratio 1:2.5:1:0.5 immediately before determinations (e.g. 50 mL ammonium molybdate, 125 mL sulfuric acid, 50 mL ascorbic acid, and 25 mL potassium antimonyl-tartrate). Ammonium Molybdate solution: dissolved 15 g $(NH_4)_6Mo_7O_{24}{\cdot}4H_2O$ in 500 mL of Nanopure water, stable at RT in a plastic bottle. Sulfuric acid solution: added 140 mL concentrated H_2SO_4 (specific gravity 1.82 g/mL) to 900 mL with Nanopure water. Ascorbic acid solution: dissolved 27 g ascorbic acid in 500 mL (stable for 1 week at RT, can be frozen). Potassium antimonyl-tartrate solution: dissolved 0.34 g of $KSbC_4H_4O_7{\cdot}1/2H_2O$ in 250 mL of Nanopure water (solution stable at RT). Readings at A_{885} were taken after incubation for 1.5 h, at RT.

Nitrate levels in the medium, referred to as Dissolved Inorganic Nitrogen (DIN, μM), were determined in filtered endpoint medium (prepared as above) by measuring A_{220} in 0.2 mL vol. in UV-transparent assay plates (Fisher) or 0.6 mL in (2 mm) quartz cuvettes (Collos et al., 1999).

Cellular measurements

Cell counts and cell diameter (single cells) were determined by Coulter counter (Beckman Coulter) and microscopy with a Neubauer haematocytometer (following Lugol staining) using a 100 X objective for cell diameter, with images processed with ImageJ.

QUANTIFICATION AND STATISTICAL ANALYSIS

Multivariate analysis

Response Surface Methodology (RSM) was carried out using Design Expert 10 (Stat-Ease), modeling storage production rates based on input variables of incident light; CO_2 supply concentration; replacement medium nitrate (N_s) and phosphate (P_s) concentrations, and operational rate (OR) where the latter was the product of μ_{MAX} and $\%\mu_{MAX}$. Correlation matrix PCA analyses were carried out with the above inputs, using $\%\mu_{MAX}$ rather than OR, by employing PAST (Hammer et al., 2001). Daily nitrate (N_i) and phosphate (P_i) supply rate terms were defined as the product of N_s (or P_s) and the replacement vol./culture vol. ratio. Under semi-continuous culture, growth rate was defined as the biomass productivity (BMP), which was

determined as the dry biomass concentration at endpoint multiplied by the replacement vol./culture vol. ratio. The oil productivity proxy TFP was defined as the product of BMP and endpoint biomass TFA content, similarly for carbohydrate (CHP) and protein (PRP). Regression analyses in the form of contour plots and heat maps were generated using NCSS 12 (NCSS statistical software). Other regression plots and curve fittings were carried out in Microsoft Excel and matrices of correlation coefficients were generated using PAST (Hammer et al., 2001). Significance was determined using Paired 2-tail t-tests which were carried out in Microsoft Excel. Further graphical displays and analyses were carried out using MATLAB.

Threshold breakpoints

Threshold breakpoints were estimated from turning points of 4^{th} order polynomial curve fitting equations and the choice of this curve is discussed in Figure S14. At the turning points, the differentiated equation (a 3^{rd} order polynomial) equated to zero and this was solved for the abscissa using WolframAlpha software (Wolfram). Threshold breakpoints were also estimated from the contour boundaries of storage-product induction zones created by 2-D regression heat maps (NCSS 12, NCSS statistical software).